MASTER IN MATHEMATICS RESEARCH FOCUS

Generation of an ABCB5-knockout human melanoma cell line using the CRISPR/Cas9 genome editing-tool
Study of ABCB5 subcellular localization by cell fractionation

Guerit, Emilie

Award date:
2019

Awarding institution:
University of Namur

Faculté de Médecine

Generation of an ABCB5-knockout human melanoma cell line using the CRISPR/Cas9 genome editing-tool - Study of ABCB5 subcellular localization by cell fractionation

Mémoire présenté pour l'obtention

du grade académique de master en sciences biomédicales

Emilie Guérit

Janvier 2019

Université de Namur
FACULTE DE MEDECINE
Secrétariat des départements
Rue de Bruxelles 61 - 5000 NAMUR
Téléphone: + 32(0)81.72.43.22
E-mail: manon.chatillon@unamur.be - http://www.unamur.be/

Generation of an ABCB5-knockout human melanoma cell line using the CRISPR/Cas9 genome editing-tool - Study of ABCB5 subcellular localization by cell fractionation

Emilie Guérit

ABC transporters are integral membrane proteins mediating the active transport of molecules towards the plasma membrane and playing a role in a wide variety of physiological functions of the cell. Many of these transporters are also implicated in cancer drug resistance. ABCB5 has been described as a marker of skin progenitor cells, melanoma stem cells, and limbal stem cells. It was reported to be a mediator of multidrug resistance in many cancers including melanoma. More recent data also suggest a role of ABCB5 in tumor development and progression. Although eleven transcripts of human ABCB5 have been identified, including two long transcripts named ABCB5FL (full-length) and ABCB5*β*, the transporter remains little characterized and its subcellular localization has not been validated yet. This research project is divided in two parts. First, it aims to generate an ABCB5-knockout human melanoma cell line to create a powerful tool better characterize the ABCB5 transporter. Second, it aims to use this ABCB5-knockout cell line to pursue the study of the ABCB5 subcellular localization. The CRISPR/Cas9 genome editing tool will be employed to knockout the *ABCB5* gene, by removing either a fragment of 53 kb or 125 kb. For that purpose, high quality guide RNAs will be selected to target specific regions of the gene and to limit the risk of off-target effects. The ABCB5-knockout cell lines will be validated at the genomic level by PCR and sequencing, and at the proteic level by Western Blot. The latter will also serve to prove the specificity of the anti-ABCB5 antibodies. The method of cell fractionation described by de Duve *et al.* will be used to study the ABCB5 subcellular localization.We successfully obtained cell lines with a biallelic 53 kb deletion and cell lines with a monoallelic 125 kb deletion in *ABCB5*. Both have been validated at the genomic level by PCR and sequencing, and the proteic validation is being performed. We performed a first set of cell fractionation on the Mel-Juso parental cell line to optimize the method and to establish a first distribution profile of ABCB5. Although we have detected an enrichment of ABCB5 in the nuclear and microsomal fractions, our results remain hypothetical. Indeed, the anti-ABCB5 antibody used in the experiment is a polyclonal antibody, which recognizes many other proteins. After validating the specificity of the antibody by Western Blot, we will perform a second fractionation on both ABCB5-expressing and ABCB5-knockout Mel-Juso cell lines to strenghten the current data on the transporter localization.

Keywords: ABCB5 transporter, CRISPR/Cas9, knockout, characterization, localization

Mémoire de master en sciences biomédicales

Janvier 2019

Acknowledgments

Firstly I would like to thank Pr. Gillet for his welcome in the LBMC laboratory.

Thanks to Marie, Géraldine, Laurent, and Florence for their tips and learning of all laboratory practices. Thanks to them, Louise, and Miguel for all the good moments during these ten months in the office.

Thanks to Olivier for his help to optimize the CRISPR/Cas9 method, and thanks to the laboratory of Pr. Debacker for the loaned material.

Thanks to the laboratory of Pr. Jadot and to Virginie for the subcellular fractionation.

Thanks to my sister Stéphanie for reading and giving me advice to write my Master Thesis. Thanks to my parents and my sister Laure for their support and encouragement during my studies.

Abbreviations

ABC ATP binding cassette
ATP Adenosine triphosphate
BCRP Breast cancer resistant protein
BRET Bioluminescence Resonance Energy Transfer
BSA Bovine serum albumin
CDKN2a Cyclin-dependent kinase Inhibitor 2A
CFTR Cystic Fibrosis Transmembrane Conductance Regulator
CRC Colorectal cancer
CRISPR Clustered Regularly Interspaced Short Palindromic Repeats
CSD Chronically sun damage
CTLA-4 Cytotoxic T-lymphocyte-associated protein 4
CXCR1 C-X-C motif chemokine receptor 1
DMEM Dulbecco modified eagle medium
DMSO Dimethyl sulfoxyde
DNA Deoxyribonucleic acid
DSB Double-strand break
DTIC Dacarbazine
EDTA Ethylenediaminetetraacetic acid
EGF Epidermal growth factor
FACS Fluorescence-activated cell sorting
FL Full-length
FSC Forward scatter
GDLP1 Glycerol-3-phosphate deshydrogenase 1 like
GDP Guanosine diphosphate
GFP Green fluorescent protein
GTP Guanosine triphosphate
HDL High-density lipoprotein
HDR Homology directed repair
HIF-1α Hypoxia-inducible factor 1-alpha
IFN Interferon
IL Interleukin
KNL1 Kinetochore scaffold 1
KO Knockout
LB Lysogeny broth
MAPK Mitogen-activated protein kinase
MDR Multidrug resistance
MIT Massachusetts Institute of Technology
MMIC Malignant melanoma iniating cell
MRP Multidrug resistance-associated protein
NHEJ Non homologous end-joining
NF1 Neurofibromin 1
NF-κ**B** Nuclear factor-kappa B
ORC3 Origin recognition complex subunit 3
PAM Protospacer adjacent motif

PBS Phosphate buffered saline
PCR Polymerase chain reaction
PD1 Programmed cell death 1 protein
PFKP Phosphofructokinase platelet
PI3K Phosphoinositide 3-kinase
PIP3 Phosphatidylinositol (3,4,5) triphosphate
PTEN Phosphatase and tensin homolog
PVDF Polyvinylidene difluoride
RFU Relative fluorescence unit
RGP Radial growth phase
RHOV Ras homology family member V
RNA Ribonucleic acid
RSS Relative specific signal
RT Room temperature
RT-qPCR Real-time PCR
SDS Sodium dodecyl sulfate
siRNa Small interference ribonucleic acid
SRA Specific relative activity
SSC Side scatter
STYK1 Serine/threonine kinase 1
TALE Transcription activator-like effector
UV Ultra-violet
VAT1L Vesicle amine transport 1 like
VGP Vertical growth phase
WT Wild-type
ZF Zinc finger

Contents

Introduction

1. ABC transporters

The ABC transporters are integral membrane proteins that constitute the largest family of transmembrane proteins. They are found in both prokaryote and eukaryote species, in which they mediate the active transport of a variety of molecules across the plasma membrane [1, 2]. These transporters are called primary transporters as the source of energy required for the transport of molecules against their chemical gradient is provided by an enzymatic reaction, *i.e*, the hydrolysis of adenosine triphosphate (ATP) [2].

ABC transporters are categorized as importers or exporters, depending on the direction of the substrate transport in- or outside the cytoplasm [3]. Exporters are common to all species, but importers are only found in bacteria in which they drive the import of essential compounds that cannot diffuse across the cell membrane such as: sugars, vitamins, metal ions, etc. [1]. In eukaryotic cells ABC transporters export a range of diverse substrates from simple ions to more complex molecules (*e.g.*, peptides, lipides, hydrophobic and organic compounds, etc.) [3, 4].

In human, the ABC transporters play a role in many biochemical and physiological processes to maintain cell homeostasis. Furthermore, theyalso able to mediate cancer multidrug resistance (MDR) either in sequestering drugs in organelles or in transporting them out of the cell. Finally, there is a growing body of evidence to support a role of ABC transporters in tumor biology, which has to be furtherunderstood [3, 4].

1.1 Structure

The typical structure of a full ABC transporter is represented in **Figure 1** and consists of two transmembrane domains (TMDs) and two nucleotide binding domains (NBDs).

The NBDs are located in the cytoplasm and bind ATP. These domains provide the energy required for the transport of the substrate against its chemical gradient by the hydrolysis of ATP. The NBDs contain two highly conserved sequences among the majority of ATP-binding proteins, *i.e.*, the Walker A and B motifs [1]. In addition, they also contain the Q-loop that couples the NBD and the TMD together, the H-loop, the D-loop, and the short sequence LSGGQ, specific of ABC transporters and involved in nucleotide binding [2].

Each TMD is composed of six hydrophobic α-helices forming a transmembrane pore. Unlike the NBDs, the TMDs do not present any conservative sequence among all ABC transporters. This property is due to the domain function that consists in determining substrate transport specificity. However, the members of a same family of transporters share a similar topology and have a range of substrates closely related [2].

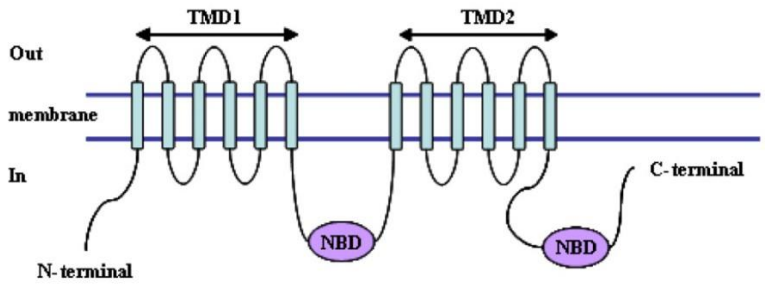

Figure 1: Structure of a full ABC transporter. The conventional topology consists of two transmembrane domains (TMDs), each of them composed of six α-helices, and responsible for substrate transport specificity; two nucleotide binding domains (NBDs) for ATP binding. Figure adapted from Gillet *et al.* [5].

Some ABC transporters also exist as half transporters or as full transporters with an additional TMD at the amino-terminal side of the protein (**Figure 2**). Among those, ABCC1, C2, C3, and C6 are full transporters that contain an additional domain composed of five α-helices at the amino-terminal end. ABCB2, B3, B6 to B10, and ABCD1 to D4 are half transporters. These half transporters consist of one TMD and one NBD located at the carboxy-terminal side of the TMD. Finally, the ABCG family members are reverse half-transporters, *i.e.*, with the NBD located at the amino-terminal side of the TMD. The half-transporters alone are not functional, and must homo- or heterodimerize to be functional [5].

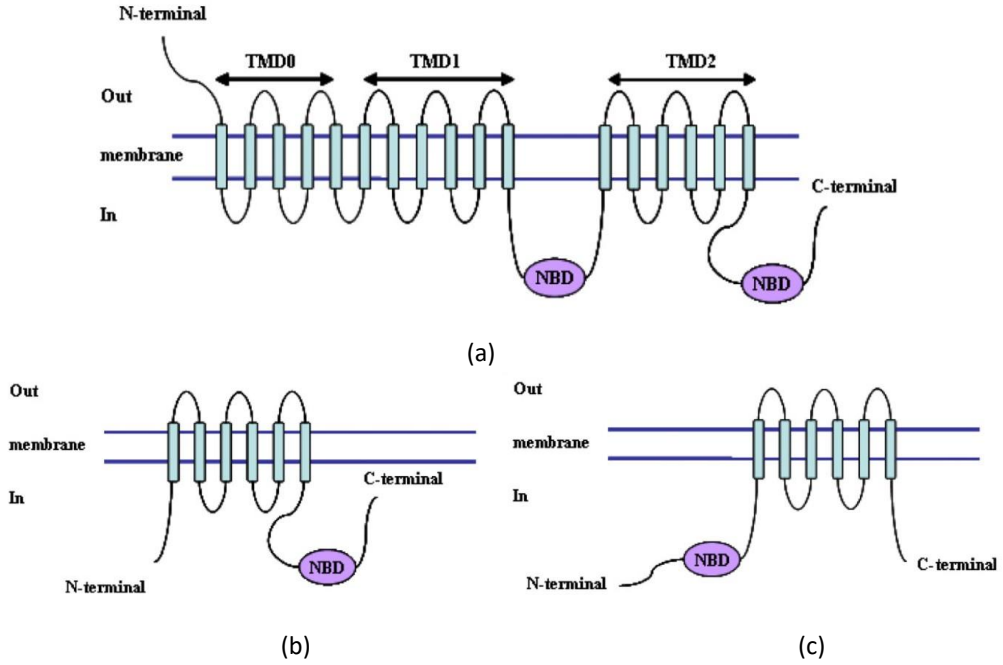

Figure 2: Additional structures of ABC transporters (a) Structure of ABCC1, C2, C3, and C6. All are full transporters with an additional domain composed of five transmembrane segments. (b) Structure of ABCB2, B3, B6 to B10, and ABCD1 to D4. All are half-transporters with one transmembrane domain (TMD) and one nucleotide binding domain (NBD) located at the carboxy-terminal side of the TMD. (c) Structure of ABCG transporters as reverse half-transporters, *i.e.*, with the NBD located at the amino-terminal side of the TMD. Figure adapted from Gillet *et al.* [5].

1.2 Catalytic cycle

The majority of ABC transporters mediate the transport of substrates against their chemical gradient. This process requires a source of energy, which is provided by the hydrolysis of ATP [2]. Several models have been proposed to explain the catalytic cycle of ABC transporters. Although different, all of them describe some fundamental steps as shown in **Figure 3**. The substrate binds to the TMDs and two ATP molecules bind to the NBDs. This is followed by the hydrolysis of one ATP molecule, which results in the conformational change of the TMDs, allowing the release of the substrate from the transporter. The second molecule of ATP is then hydrolyzed for the reset of the transporter [6].

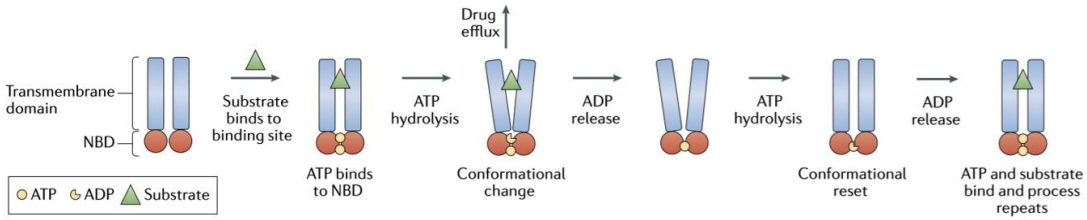

Figure 3: Schematic representation of ABC transporter catalytic cycle. The substrate binds to the transmembrane domains (TMDs) and two ATP molecules bind to the nucleotide binding domains (NBDs). First ATP hydrolysis results in the conformational change of the TMDs followed by the substrate release from the transporter. Second ATP hydrolysis allows the reset of the transporter. Figure adapted from Robey *et al.* [6].

1.3 Families and functions

In human, 48 ABC transporters exist. They are classified into seven families denoted by A to G. This subdivision is based on similarities shared by each family member: gene structure, order of the domains, and sequence homology in the NBDs and the TMDs domains [1, 3].

The ABCA family contains the largest ABC genes. These genes code for 12 full transporters which are mainly implicated in lipid trafficking [3]. Among all the ABCA family members, ABCA1 and ABCA4 are the best described. ABCA1 mediates the cellular efflux of phospholipids and cholesterol. Mutations in the gene are reponsible for disorders of cholesterol transport and of high density lipoproteins (HDL) synthesis. ABCA4 transports vitamin A derivatives in photoreceptor cells and plays an important role in the visual cycle [1, 7].

The ABCB family is also called the "Multidrug resistance (MDR) family" as several members are involved in the mechanism of multidrug resistance against a wide range of compounds. The ABCB transporters are unique to the mammal species and consist of 11 genes coding for four full-transporters and seven half-transporters. ABCB1 (also known as p-glycoprotein or MDR1) has been studied for a long time and was the first human ABC transporter cloned and characterized by Riordan *et al.* in

1985 [8]. ABCB1 is widely expressed in the intestinal epithelium, in liver cells, in the cells of the proximal tubule of the kidney, but also in endothelial cells of the blood-brain barrier and the blood-testis barrier. It principally works as drug efflux pump of a broad range of xenobiotics to protect cells against intracellular drug accumulation [9]. ABCB2 and ABCB3 both encode half-transporters. They heterodimerize and mediate the transport of peptides into the endoplasmic reticulum. ABCB4 and ABCB11 are localized in the liver and implicated in the secretion of bile acids. ABCB6, ABCB7, ABCB8, and ABCB10 miss an amino-terminal domain. They are expressed in the mitochondria where they contribute to iron metabolism. Finally the ABCB9 half-transporter has a broad expression in testis, in which the precise function remains unclear [10]. The ABCB5 transporter will be further described (**Section 3**).

The ABCC family, also called the "Multidrug resistance-associated protein (MRP) family", encodes 12 full-transporters. ABCC1, ABCC2, and ABCC3 mediate the transport of drug conjugated to glutathione and other organic anions [1]. ABCC4 (MRP4), ABCC5 (MRP5) are smaller proteins missing an amino-terminal domain. Both transporters act as efflux transporters of small molecules involved in cellular signaling (*e.g.*, nucleotides, eicosanoids, etc.) [11]. The ABCC7, known as Cystic Fibrosis Transmembrane Conductance Regulator (CFTR) is particular. It has the common architecture of the majority of ABC transporters, but it does not mediate the active efflux of molecules: it is a chloride ion channel that allows the transepithelial movement of salt and liquid and that plays a role in exocrine secretions [1, 12, 13]. Finally, ABCC8 and ABCC9 mainly found in endocrine cells and neurons. They form a complex with potassium channel subunits and contribute to the regulation of insulin secretion and glucose homeostasis [4, 14].

The ABCD family members are also called "peroxisomal ABC transporters". The *ABCD* genes encode four half-transporters that play a role in very long chain fatty acid oxidation in the peroxisome [1, 3].

The ABCE and ABCF families consist of proteins that do not function as transmembrane transporters. The genes code for the NBDs common to others ABC transporters, but lack the TMDs which are crucial to function as transporters. The ABCE family only contains ABCE1, an oligo-adenylate binding protein which promotes interferon activity in response to some viral infections. The ABCF family member ABCF1 is associated with ribosomes and regulate the innate immune response [1, 15].

The ABCG family is composed of six "reverse" half-transporters, *i.e.*, with the NBD located at the amino terminal side of the TMD. These transporters must homo- or heterodimerize to form functional transporters. ABCG1 is mainly expressed in adipocytes and macrophages, in which it regulates cholesterol transport [1, 3, 16]. ABCG2, also known as the breast cancer resistant protein (BCRP), is located in the apical membrane of hepatocytes, epithelial cells of the small and large intestines, and ducts and lobules of the breast. It forms a homodimer and mediates the transport of steroids, bile acids, and toxins to facilitate their elimination [16]. The functions of ABCG3 and ABCG4 are still unclear. ABCG3 is mainly found in the thymus and spleen where it could transport specific peptides or hydrophobic compounds from lymphocytes [3]. ABCG4 might heterodimerize with ABCG1 and thereby might be

involved in cholesterol transport [16]. Finally, ABCG5 and ABCG8 are transporters of sterols. They limit their intestinal absorption and increase their biliary excretion [3].

1.4 Role in cancers

These past few years, the interest in studying the role of ABC transporters in cancers has grown. It is well recognized that they are involved in the mechanism of cancer multidrug resistance by mediating the efflux of anticancer drugs out of the cell or their sequestration in organelles. However, recent studies indicate that the loss or inhibition of ABC transporters may influence cancer cell phenotype through modifications in cell proliferation, differentiation, invasion, and migration. These report suggest an additional drug efflux-independent role of ABC transporters in tumor biology that remains to be further understood [17, 18].

1.4.1 Multidrug resistance

The multidrug resistance is defined as a cell that became resistant not only to the compound that was initially administered, but also to a wide range of compounds that are structurally and mechanistically unrelated [6]. This is one of the major mechanisms thatcauses chemotherapy failure. Each year, it leads to the death of many patients affected with metastatic cancer [1, 6].

ABCB1 is overexpressed in different subtypes of kidney, colon, breast, and lung cancers [19, 20]. It confers cancer cells resistance by the efflux of a range of anticancer drugs such as anthracyclines, vinca alkaloïds, and taxanes [21]. ABCC1 was cloned for the first time in 1992 by Cole and colleagues, who demonstrated that the transporter was able to confer resistance to doxorubicin, etoposide, vincristine, and methotrexate. The transporter is overexpressed in several cancers including lung, breast, prostate, and childhood neuroblastoma, but its precise role in the mechanism of MDR remains unclear [6]. Finally, ABCG2 is overexpressed in multiple solid tumors and hematological malignancies showing resistance to anthracyclines [6]. However, it is unclear if ABCG2 is responsible of the resistance to antracyclines observed in these types of cancers. Studies suggest that ABCG2 could be a marker of the subpopulation of chemoresistant cells rather than a direct contributor to this phenotype [22, 23].

1.4.2 Tumorigenesis

The role of ABC transporters in cancer biology is still little understood. However, there is a growing body of evidence that the ABC transporters possess an additional drug efflux independent role in tumorigenesis [23, 24, 25]. Several experiments on mice models show that the disruption of some ABC transporters alter the tumorigenesis. The first study was performed by Mochida *et al.* on a mouse model of colorectal cancer. They knockout the *Abcb1* gene and observed a reduction in the number of intestinal polyps and tumour incidence [26]. More recently, the role of some ABCC family members in neuroblastoma genesis has been investigated. Henderson *et al.* show that the disruption of *Abcc1* in a mouse model of neuroblastoma decreases tumor incidence and increases tumor latency. In addition, they performed a series of *in vitro* assays on neuroblastoma cells to analyze the role of ABCC1, C3, and C4 in tumor biology. They identified that the overexpression of ABCC1 may increase cell

migration and colony formation. The expression of ABCC4 promotes cell proliferation and clonogenicity.A low expression of ABCC3 is associated with tumor recurrence or death [25]. Finally, some ABC transporters are also associated with poor patient outcome in advanced epithelial ovarian cancer. Among those, Hedditch *et al.* show that high levels of ABCA1 in primary tumors significantly correlate with a decrease in patient overall survival. These data are supported by experiments performed to silence the ABCA1 expression in human ovarian cancer cells. The results show that this inhibition prevents both cell proliferation and migration. In addition, ABCC7 expression is associated with late stage epithelian ovarian cancer. The silencing of the transporter in human ovarian cancer cell lines results in decreased cell migration, invasion, proliferation, and adhesion [27].

Although these reports show a link between ABC transporters and tumorigenesis, the deep mechanism remains obscur. Fletcher *et al.* suggest that this role is likely related to the physiological function of these transporters, *i.e.*, efflux of endogenous metabolites, signaling molecules, etc. To date, the knowledge about these specific endogenous substrates remains limited. The emergence of metabolomic studies constitutes a powerful strategy to screen and identify previously unrecognized endogenous substrates of ABC transporters to afterwards better understand their role in tumor biology [23].

2. Melanoma

Cancer is the second cause of death in Europe. Although Europe only represents 9% of the world population, 25% of the total of cancer cases occur in the continent. It is estimated that in 2018 around 3.98 million new cases of cancer will be diagnosed and that 1.93 million of patients will probably die from the disease [28].

Skin cancer is classified into three types: basal cell carcinoma, squamous cell carcinoma, and melanoma. Melanoma is a malignant neoplasm derived from melanocytes. It only represents 5% of all skin cancer cases, but its incidence has increased worldwide over the past 30 years. This type of cancer is the most aggressive form of skin cancer and is responsible for the death of many patients [29]. Ferlay *et al.* estimate that in 2018, 144,200 new cases of melanoma will be diagnosed in Europe and that around 27,100 people will die from the disease [28].

2.1 Classification

Melanoma can be subdivided into non-cutaneous and cutaneous melanoma. The first one is less common and is mainly located near the eyes and the mucosal tissues (*e.g.*, genital, anal, oral cavities, etc.). The second one is more frequent and represents around 90% of all melanoma cases [29].

Cutaneous melanoma can be distinguished between chronically and non-chronically sun damaged (CSD and non-CSD) melanoma (**Figure 4**). These two forms differ according to their anatomical site of origin, the age at onset, the level of sun

exposure, and the burden and types of mutations [30]. The vast majority of CSD melanomas affect people older than 55 years, and are mainly found in head, neck, and dorsal surface of distal extremeties (*i.e.*, sites with high levels of sun exposure). They are heterogenous tumors that carry a high degree of mutations in several genes such as: *NF1*, *NRAS*, *BRAF*, and *cKIT*. Non-CSD melanomas often originate from previous naevi. They affect young people (*i.e.*, under 55 years old) and are principally located in the trunk and proximal extremities. They show lower burden of mutations, but are frequently associated with the $BRAF^{V600E}$ mutation [30, 31].

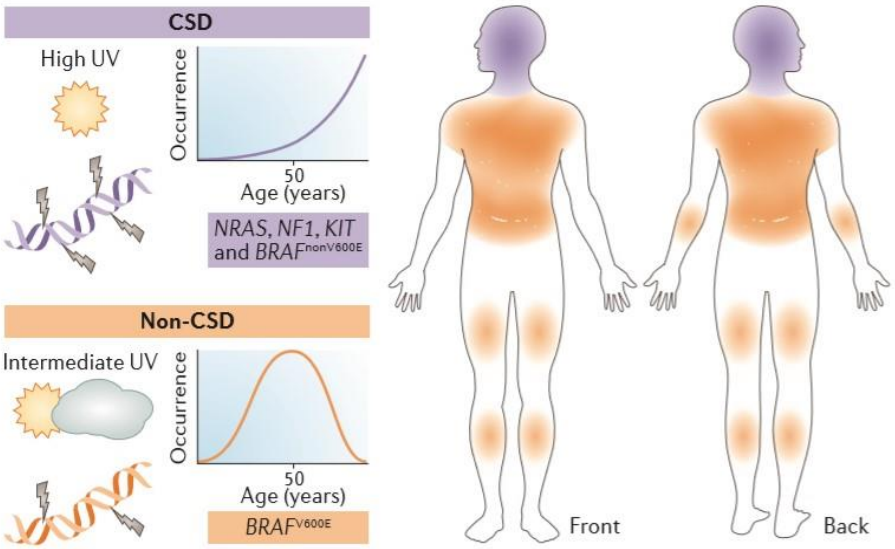

Figure 4: Classification of cutaneous melanomas into chronically and non-chronically sundamage (CSD and non-CSD) melanomas. CSD melanomas are characterized by: long-term ultraviolet (UV) radiations exposure, age of onset older than 55 years old, high burden of mutations, and major location in head, neck, and dorsal surface of distal extremities. Non-CSD melanomas mainly affect people under the age of 55, are often associated with the $BRAF^{V600E}$ mutation, and are located in the trunk and proximal extremities. Figure adapted from Shain *et al.* [30].

2.2 Risk factors

Several parameters may increase the risk of melanoma development. Among those, some environmental factors may be controlled to reduce the risk of tumour development (*e.g.*, the level of ultraviolet (UV) radiation exposure). However, others factors are directly related to host characteristics and are non-modifiable (*e.g.*, ethnicity, geography, number of naevi, family history of melanoma cases, etc.) [32].

Ultraviolet exposure is a well known environmental risk factor of melanoma development that can be controlled by the utilisation of appropriate strategies of prevention [32, 33]. There are three types of UV radiations: UV-A, UV-B, and UV-C. These subtypes differ in their radiation emission spectrum, their absorption by the ozone layer, and their penetration in the skin [34, 35]. Although UV-A and -B are the most dangerous for humans, all have genotoxic effects. Long-term sun exposure can induce DNA damages by the production of DNA adducts leading to the formation of pyrimidine dimer mutations [36].

Gender, ethnicity, and geography. Gender mainly influences the anatomic site of the tumor. In males, melanomas are usually located in the trunk. In females, they are frequently found in lower limbs [32]. In a lower extent, studies have also reported differences in the survival rate among men and women: the latters show a lower risk to develop metastases and thereby have an increased survival rate [37]. Both ethnicity and geography may influence the incidence of melanoma. The incidence is increasing among the Caucasian populations [32], with the highest rate in Australia. In contrary, melanoma are extremely rare among black populations, which is due to a greater amount of melanin that protect them from the UV-carcinogenic effects [32].

Number of naevi and family history. The number of melanocytic naevi and the family history of melanoma cases increase the risk to develop melanoma. In the first case, studies show that around 26% of melanomas arise from previously existing naevi [33, 38], and that patients with more than 100 naevi have seven-fold increased risk of melanoma development [39]. In the second case, previous history of melanoma cases in the family increases the probability to develop inherited melanoma. This subtype of cancer is characterized by germline mutations in the genes coding for proteins that regulate cell proliferation. The two most commonly mutated genes are *CDKN2a* and *CDK4*. These mutations predispose the patient to develop melanoma, particularly at a young age [38, 40].

2.3 Clark's model

Melanocytes are neural crest-derived cells located in the epidermis, hair follicles, uveal tract of the eye, meninges, and anogenital tract [30]. The physiological role of melanocytes consists in producing melanin pigments in response to UV-exposure. The synthesis of melanin is performed in specific organelles called the melanosomes. These organelles follow several steps of maturation from early melanosome (*i.e.*, without pigments) to late melanosomes (*i.e.*, with high melanin content). Late melanosomes are secreted out of the cells and are transfered to keratinocytes to protect them against UV radiation-induced DNA damages [30, 41].

The process of transformation from melanocytes to melanoma is complex and results from an accumulation of mutations in several genes. Different models exist to define the process of melanomagenesis, from a benign lesion to a more aggressive and invasive form. The Clark's model (**Figure 5**) is widely used to describe melanoma development according to the degree of tumor invasion.

The first step consists of a proliferation of melanocytes that leads to the apparition of a benign naevus. Mutations in the *BRAF* oncogene are frequently found at this stage in melanocytes and increase the rate of proliferation in this cell population. After an initial proliferation, melanocytes enter into a senescence-like state in which their probability to progress to melanoma remains very poor. Benign naevi have the tendency to involute and to disappear after the age of 50. Dysplastic naevi are classified into mild, moderate or severe lesion, depending on their risk of progression to melanoma. They are characterized by structural and cytological atypia, and by the acquisition of additional mutations to *BRAF*. Mutations in the *CDKN2a* and *PTEN* tumor suppressors are frequent and induce gene inactivation and loss of function. In

the radial growth phase (RGP), cancer cells become immortals. This step is defined as *in situ* melanoma as the cancer cells proliferation is horizontal and remains confined within or near the epidermis. *In situ* melanoma can persist during many years without progressing into an invasive state. In the vertical growth phase (VGF), the tumor invades the dermis and acquires metastatic capacity. Tumour cells gain advantages that promote their migration and invasion, such as the loss of E-cadherin function which inhibits cells adhesion. Melanoma are called metastatic melanoma once they leave the primary tumor site. Usually, tumour cells reach lymph nodes, before to disseminate in distant organs through the entire body [30, 42].

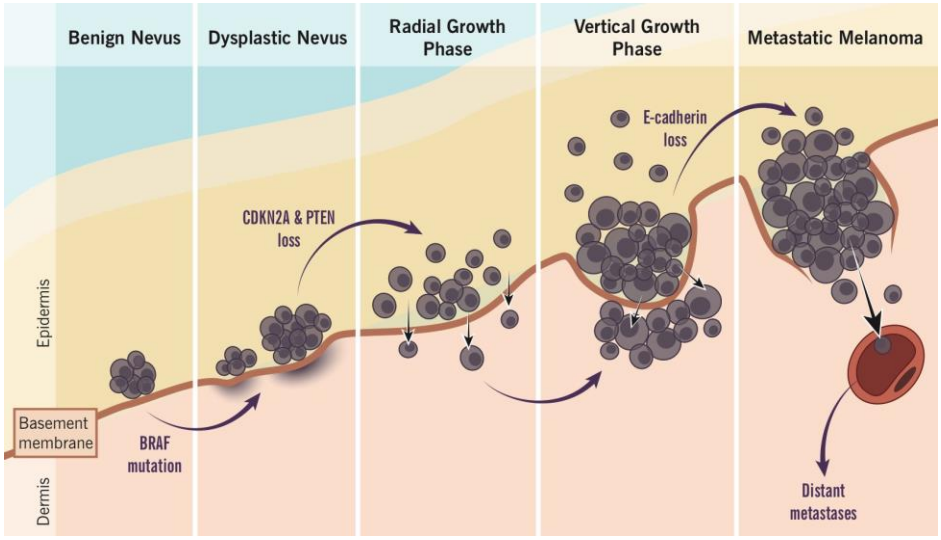

Figure 5: Clark's model of melanoma development. Benign naevus: benign proliferation of melanocytes, frequently associated with *BRAF* mutations. The probability of progression from benign naevus to melanoma remains poor. Benign naevi very often enter into a senescence-like state which is followed by their involution and disparition. Dysplastic naevi show additional mutations, structural and cytological atypia. They can be classified into mild, moderate or severe lesion, depending on the risk of progression to melanoma. The radial growth phase (RGP) (*in situ* melanoma) is described as the horizontal proliferation of melanoma cells that remains confined within or near the epidermis. This state can persist for many years without progression. In the vertical growth phase (VGP), melanoma cells invade the dermis and acquire a metastatic capacity. The loss of E-cadherin function promotes cell migration and invasion. In metastatic melanoma, the cancer cells leave the primary tumor site and reach lymph nodes, blood vessels, and distant organs through the entire body. Figure adapted from E. Wong *et al.* (http://www.pathophys.org/melanoma).

2.4 Mutations in melanoma

As mentioned above, the process of melanoma development and progression is closely related to the acquisition of a range of mutations. These mutations either activate a proto-oncogene or inactivate a tumor suppressor leading to the activation of signaling pathways promoting cell growth, proliferation, survival, migration, and invasion. The RAS-RAF-MEK-MAPK and the PI3K pathways are the most commonly upregulated signaling pathways in melanoma. In the following paragraphs are described the genes highly mutated in melanoma.

BRAF. The *BRAF* oncogene is mutated in around 40 to 60% of all melanoma cases and is considered as the most frequent somatic mutation of the malignancy. The gene codes for a serine/threonine protein kinase that belongs to the RAS-RAF-MEK-MAPK pathway. 90% of the mutations in *BRAF* result from a valine-to-glutamate change at position 600 (called the $BRAF^{V600E}$ mutant). This specific mutation constitutively activates the MAPK pathway and promotes the ERK phosphorylation. Benign naevi frequently show the $BRAF^{V600E}$ mutation. As these naevi do not present any malignant properties, it is suggested that the $BRAF^{V600E}$ mutant alone is not sufficient to induce melanocytes transformation into cancer cells [29, 36, 43, 44, 45].

NRAS. The *NRAS* oncogene belongs to the RAS family of genes. The protein is a monomeric guanosine triphosphatase located at the plasma membrane. The protein physiologically switches between two states: an active form bound to GTP and an inactive form bound to GDP. NRAS is activated after the binding of extracellular subtrates to a specific tyrosine kinase receptor (*e.g.*, c-KIT, ERBB4). NRAS may interact with several RAF proteins, which are then phosphorylated and activated. Activating mutations in *NRAS* are identified in around 20% of melanoma cases and these mutations act by keeping the NRAS protein under its GTP-bound active form. It results in a constitutive activation of both the RAS-RAF-MEK-MAPK and the PI3K-AKT pathways [29, 36, 43, 44, 45].

PI3K-AKT. The first step of the PI3K-AKT pathway consists of the production of phosphatidylinositol (3,4,5) triphosphate (PIP3) by the phosphoinositide 3-kinase (PI3K). The PIP3 activates the AKT serine/threonine kinase that subsequently promotes cell growth and proliferation. The PI3K-AKT pathway is commonly activated in melanoma and may result from activating mutations in the *NRAS* oncogene but also from the inactivation of the *PTEN* tumor suppressor. The latter physiologically mediates the dephosphorylation of the PI3K enzyme, acting as a negative regulator of all the downstream effectors. *PTEN* is mutated in 10-30% of melanoma and results in constitutive activation of the PI3K pathway in a receptor-independent way. Finally, a specific mutation (E17K) in the AKT3 isoform has been identified in melanoma cell lines, resulting in constitutive activation of the protein [29, 31, 36, 46, 45].

Neurofibromin 1 (NF1). The *NF1* gene encodes a tumor suppressor that physiologically downregulates both the MAPK and PI3K pathways. It stimulates the GTPase activity of NRAS to promote the transition from the active RAS-GTP form to the inactive RAS-GDP, acting as a negative regulator of the protein [47]. The mutations inducing loss of NF1 function prevent the regulation of NRAS and induce its constitutive activation. Mutations in *NF1* are mainly found in desmoplastic melanoma and in most cases are associated with other mutations, *e.g.*, in *BRAF* or *NRAS* [48].

Tyrosine kinase receptors. ERBB4 is a member of the ERBB/HER family of tyrosine kinase receptors. The mutations in ERBB4 increase the kinase activity, resulting in an anchorage-independent cell growth and melanoma progression. c-KIT is a tyrosine kinase receptor that plays a role in melanocytic development. Amplification in *c-KIT* have been reported in around 6-8% of different subtypes of melanoma. The role of c-KIT in melanoma remains unclear but functional analyses show that specific mutations in c-KIT may activate the PI3K pathway in normoxic

conditions and the RAS-RAF-MEK-ERK-MAPK pathway in hypoxic conditions [45, 49].

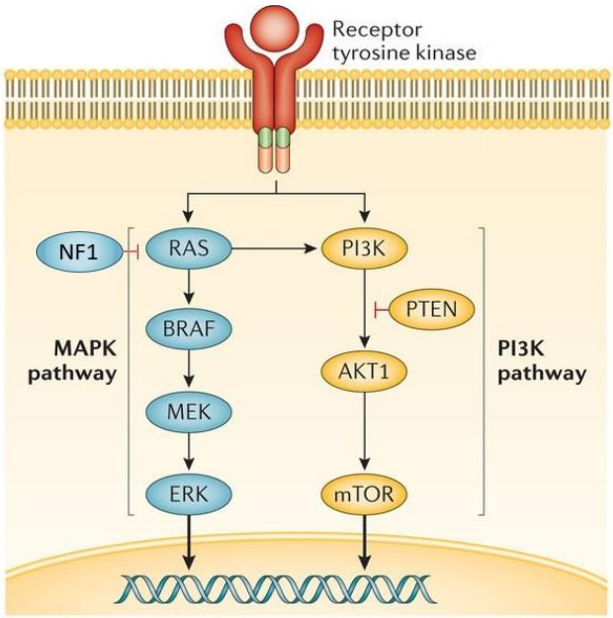

Figure 6: Main signaling pathways upregulated in melanoma. The activation of MAPK pathway results from mutation and activation of the proto-oncogenes *NRAS* or *BRAF* or mutation and inactivation of the tumor suppressor *NF1*. The activation of the PI3K/AKT pathway results from activating mutation in the *AKT* proto-oncogene or mutation and loss of function of the tumor suppressors *PTEN* or *NF1*. The upregulation of these two signaling pathways promotes cell growth, proliferation, survival, migration, and invasion. Figure adapted from Dralle *et al.* [50].

2.5 Treatment

Currently, only primary melanoma is curable and provides a five-year survival rate over 90% [29]. The standard treatment consists of the surgical removal of the primary tumor and does not require any additional therapy [29, 32]. In contrary, late-stage melanoma is more aggressive. The five-year survival rate is estimated around 5% for malignancies that have disseminated to other major organs [51]. A range of therapeutic options for the management of patients with melanoma exist and the choice of treatment depends on the stage of the tumor at the time of diagnosis [32]. However, metastatic melanoma remains difficult to treat, especially due to the development of mechanisms of resistance in tumor cells [51].

Radiotherapy. The use of radiotherapy in the management of melanoma is limited as different subtypes of melanoma are radiotherapy resistant. This resistance is due to higher abilities of cancer cells to repare the DNA damages induced after exposure to low-dose radiation [32]. Thereby, radiotherapy is only used in a few cases: either as a first-line treatment of primary melanoma to replace surgery or as adjuvant therapy after tumor removal to prevent cancer recurrence [32, 52].

Chemotherapy. Only a few number of chemotherapeutic drugs show anti-tumor effects on melanoma including dacarbazine (DTIC), platinum analogs (cisplatin, carboplatin), taxanes (docetaxel, paclitaxel), and nitrosureas [53]. The use of these

agents in the treatment of metastatic melanoma is limited due to systemic toxic effects and the development of multidrug resistance [29, 53]. Moreover, the use of chemotherapy as single therapy only shows a low response rate on patients' survival. Attempts have been carried out to combine several chemotherapy regimens to obtain better results on the overall survival rate, but no real benefits have been achieved [53].

Immunotherapy. Research in the field of immunotherapy has grown very fast these past few years. This kind of therapy is particularly promising in the management of patients with melanoma because the malignancy is considered as one of the most immunogenic malignancies. Many efforts are underway to modulate and boost the patient's immune system by targeting key molecules in the regulation of the immune response [32, 54].

The interferon-α (IFN-α) drug is a mixture of proteins with anti-tumor properties such as antiangiogenic, differentiation-inducing, pro-apoptotic, antiproliferative effects, etc. [55]. In 1986, the Food and Drug Administration (FDA) approved the use of this drug as adjuvant therapy in the treatment of melanoma [32]. However, as IFN-α seems to be only effective in a subset of patients, there are now many controverses about the real benefits to use this drug in the management of melanoma [51, 55].

The administration of high dose of interleukin-2 (IL-2) was approved by the FDA in 1998 for the management of patients affected with distant metastatic melanoma. IL-2 works as a stimulator of T-cells function and proliferation. When activated, T-cells induce a specific immune response that promotes melanocytes apoptosis [32]. However, IL-2 presents high level of toxicity throughout the entire body, limiting the use of IL-2 only on patients likely to respond well to the treatment [56]. Clinical trials are underway to use alternative cytokines such as IL-15 and IL-21. These cytokines act in a similar way than IL-2 but show lower burden of toxicity.

Since 2011, three immune checkpoint inhibitors (*i.e.*, ipilimumab, pembrolizumab, and nivolumab) have been approved by the FDA for the management of unresectable or mestastatic melanoma [57]. These drugs have been successfully assessed in clinical trials. Treated patients show durable anti-tumor response and an increase in the overall survival rate [31]. These checkpoint inhibitors bind and blockade either the cytotoxic T-lymphocyte-associated protein 4 (CTLA-4) (ipilimumab) or the programmed cell death 1 protein (PD1) (pembrolizumab and nivolumab). As CTLA-4 and PD1 are important negative regulators of T-cells immune function, their inhibition results in increased activation of the immune system [32, 58].

Targeted therapy. As previously described (**Section 2.3**), melanoma is widely associated with mutations in the *BRAF* proto-oncogene, and in most cases with the $BRAF^{V600E}$ mutant [59]. It has led to the development of small inhibitors designed to target the BRAF protein and to prevent the activation of all its downstream effectors [32]. Three generations of inhibitors have been developed. The first generation showed a lack of specificity for the $BRAF^{V600E}$ mutant, but the improved design of the next generations of inhibitors improved the survival rate in many patients. The major failure in targeted therapy is that cancer cells become resistant to the inhibitors indecreasing their long-term benefit and limiting their use in monotherapy. It is suggested to use a

combination of multiple inhibitors (*e.g.,* BRAF and MEK inhibitors) as standard targeted therapy in patients with $BRAF^{V600E}$ positive metastatic melanoma [31, 60].

2.6 Drug Resistance

During these past 30 years, there has been many advances in the diagnosis and in the management of melanoma thanks to the development of targeted therapies. Despite these advances, the prognosis of the malignancy remains poor and a lot of patients die because of tumor recurrence or dissemination throughout the body [51]. One of the major cause is the resistance of cancer cells to a wide range of anti-cancer drugs. This resistance may be either intrinsic (*i.e.,* already present before the begining of the treatment) or extrinsic (*i.e.,* arriving later during the course of the treatment) [31].

Chemotherapy is usually ineffective in the management of melanoma as the malignancy is resistant to the majority of chemotherapeutic agents. This chemoresistance may result from increased abilities of DNA repair, dysregulation of apoptotic pathways, but also from the expression of drug efflux transporters on the plasma membrane [51, 61]. These mediate the efflux of drugs out of the cell, reducing their intracellular accumulation, and limiting their cytotoxic effect. Melanoma cells may express on their plasma membrane many ABC transporters including ABCB1, ABCC1, ABCA9, ABCB5, ABCB8, ABCD1, and ABCG2 [61, 62]. Although several of these transporters (*e.g.,* ABCB1) are well described as major mediators of chemoresistance in different subtypes of cancers, this specific role in melanoma remains uncertain [63, 64]. However, a particular interest was given on ABCB5, which was shown to be predominantly expressed in pigmented cells. This transporter was shown to be a marker of melanoma-initiating cells, and to have a role in melanoma drug resistance and melanoma development (**Section 3.3**).

The resistance to targeted therapies is another common failure in the treatment of melanoma. The intrinsic resistance to targeted therapy may result from already existing mutations in other genes than the targeted one. These mutations allow the cells to escape to the effect of the inhibitor. In addition, tumor cells may become resistant later during the course of the treatment. Palmieri *et al.* [31] described two distinct mechanisms to explain the acquired resistance. The first one, also the main cause of resistance to BRAF inhibitors, consists in reactivating the MAPK pathway. It may results from MEK-activating mutations, $BRAF^{V600E}$ splicing variants, etc. The second mechanism of acquired drug resistance is MAPK-independent and is due to the activation of alternative signaling pathways that also control and promote cell proliferation [31].

3. ABCB5

The ABCB5 transporter is a member of the B family of ABC transporters, predominantly expressed in pigmented cells (*i.e.* melanocytes, testis, and retinal pigmented epithelium). The transporter has been shown to be a marker of skin progenitor cells, melanoma stem cells, and more recently of limbal stem cells. It is also

reported to be a mediator of multidrug resistance in melanoma, colorectal cancer, hepatocellular carcinoma, and in several hematological malignancies [65-71]. More recently, studies suggest that beyond its role in chemoresistance, ABCB5 could also be involved in the tumor development and progression [65, 68, 72-75].

3.1 Structure

The *ABCB5* gene is located on chromosome 7p21. Studies reveal that at least 11 transcript variants of ABCB5 exist, among those three have been well documented: ABCB5 full-length (FL), ABCB5*β*, and ABCB5*α* [76].

The ABCB5FL has 28 exons and 1257 amino acids (aa). Kawanobe *et al.* performed analysis of the tissue expression level of the full length isoform. They revealed that the ABCB5FL transporter is solely expressed in prostate and testis [21]. The topology of ABCB5FL (**Figure 7(a)**) is described as the conventional structure of the majority of all ABC transporters. It consists in two transmembrane domains (TMDs), each of them composed of six *α*-helices, and two nucleotide binding domains (NBDs) for the binding and hydrolysis of two ATP molecules [76]. Other studies identified additional functional domains that consist of 14 N-glycosylation sites. Among these sites, two are located in the extracellular loop of the transporter and may play a role for the trafficking of the protein to the plasma membrane [76]. Phylogenetic and bioinformatic studies show that the full-length isoform has retained the conservative domains common to all ABC transporters throughout the entire mammalian evolution, suggesting that the ABCB5 full-length isoform corresponds to the functional form of ABCB5 [76].

The ABCB5*β* isoform contains 19 exons and 812 aa. It is predominantly found in melanocytes and other types of pigmented cells, and is highly expressed in melanoma. The predicted topology of the *β* isoform (**Figure 7(b)**) corresponds to a "half-transporter like" structure which is composed of one TMD flanked by two NBDs. This feature is atypical for a half-transporter that normally possesses only one NBD. However, one of the two NBD lacks the Walker A motif, preventing the binding of one ATP molecule. This property suggests that the half-transporter alone is not functional. These data are supported by the presence of dimerization motifs (called coil-coiled regions) in the N-terminal region of ABCB5, indicating that the *β* isoform might homo- or heterodimerize to create a functional transporter [21, 76]. Our laboratory has just recently demonstrated with the technique of Bioluminescence Resonance Energy Transfer (BRET) that ABCB5*β* may at least heterodimerize with the B family members ABCB6 and B9. Finally, Moitra *et al.* has identified six N-glycosylation sites. Similarly to those found in ABCB5FL, they could be important for the transport of the protein to the plasma membrane.

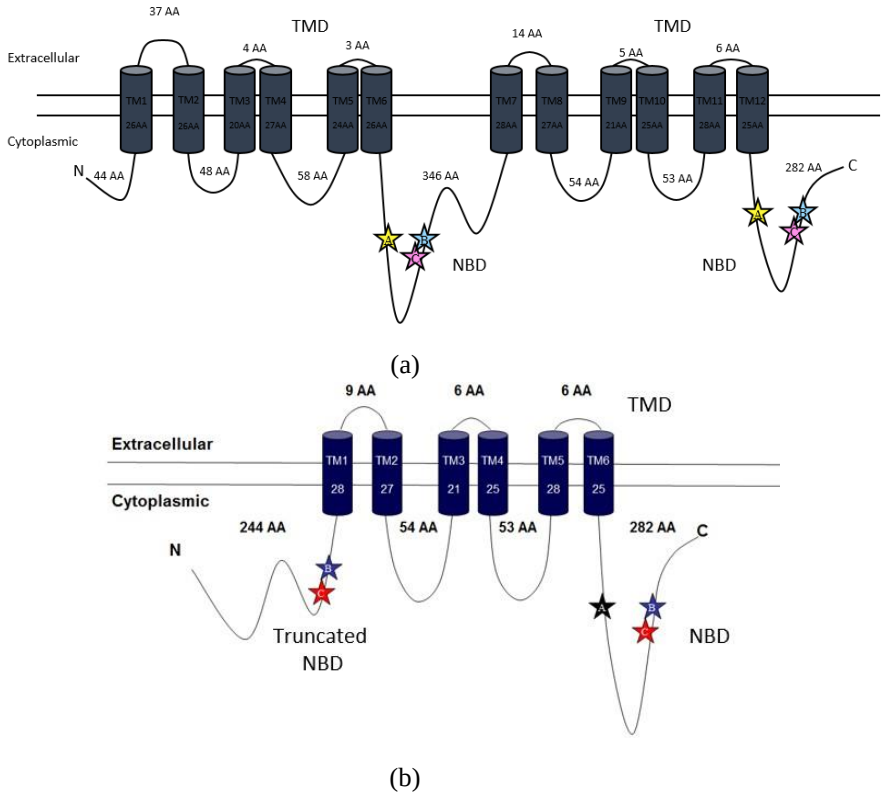

Figure 7: Structural topology of ABCB5FL and ABCB5*β* (a) Structure of ABCB5 full length: two transmembrane domains (TMD), each of them composed of six *α*-helices, and two nucleotide binding domains (NBD) for the binding and hydrolysis of two ATP molecules. (b) Half-transporter like structure of ABCB5*β* isoform: one TMD with six *α*-helices flanked by two NBDs instead of one as it would be expected for a conventional half-transporter. Figure adapted from Gillet *et al.* [5].

The ABCB5*α* form is a small soluble protein of 131 aa. This isoform has an expression profile similar to the *β* isoform both in normal and cancerous cells. Although the studies on this protein are sparse, it seems that it acts as a regulator rather than an efflux transporter [21, 76].

3.2 Role in cancers

As mentioned above, ABCB5 is overexpressed in a number of cancers such as melanoma, breast cancer, colorectal cancer, hepatocellular carcinoma, and several hematological malignancies [76]. To date, ABCB5 has been characterized as a gene mediating multidrug resistance in human melanoma, hepatocellular carcinoma, and colorectal cancer (CRC) [68]. In these cancers, the transporter is preferentially expressed by a subpopulation of $CD133^+$ cancer stem cells which show resistance to the majority of chemotherapy regimen (*e.g.*, 5-fluorouracil in CRC). ABCB5 also serves as biomarker of this cancer stem cells population and is an indicator of tumor recurrence and poor survival [68]. Beyond the implication of ABCB5 in MDR, there is a growing body of evidence that support a role of the transporter in tumorigenesis, independent from its function as drug efflux transporter [6]. In 2011, Wilson *et al.* identified a drug efflux independent role of ABCB5 in CRC, promoting more efficient tumor growth and progression [68]. This role in CRC tumorigenesis was further investigated in 2018 by Guo *et al.*. They studied the effects of either the knockdown

of *ABCB5* gene expression or the inhibition of transporter activity on tumor progression. The results show that tumor progression decreases when ABCB5 expression is downregulated and when the transporter activity is blocked, compared to the ABCB5 wild-type condition. They suggest that the transporter partly controls cell invasion, but the full mechanism remains unclear.

3.3 Role in melanoma

The interest to study ABCB5 has grown these past few years as it is amongst the most frequently mutated gene in melanoma [77, 78]. The role of ABCB5 in the mechanism of melanoma multidrug resistance is relatively well understood but its role in tumor development and progression is unclear and controversial. First reports describe that ABCB5 promotes tumor progression, invasion, and metastases [74]. However, more recent analyses performed by Sana *et al.* suggest that ABCB5 acts as a tumor suppressor and prevents tumor initiation through the inhibition of cell proliferation [78].

3.3.1 Multidrug resistance

ABCB5 preferentially marks a subpopulation of $CD133^+$ malignant melanoma-initiating cells (MMICs). These cells present a stem cell phenotype: unlimited self-renewal capacity, tumor-propagating abilities, but also multidrug resistance. For the latter, MMICs have shown to be insensitive and resistant to a range of anticancer drugs such as camptothecin, doxorubicin, paclitaxel, docetaxel, etc. There is a strong body of evidence of an involvment of ABCB5 in this mechanism of multidrug resistance by the efflux of these drugs out of the cell [74]. This role is supported by additional studies performed by Huang *et al.* who showed that the inhibition of ABCB5 through small interference RNA (siRNA) increases the cancer cells sensitivity to camptothecin [79].

3.3.2 Tumorigenesis

A role of ABCB5 in promoting tumor growth, progression, and metastases has been described in malignant melanoma-initiating cells (MMICS). Wang *et al.* performed *in vitro* experiments on $ABCB5^+$ MMICs and on $ABCB5^-$ melanoma cells and their results showed higher cell migration and invasion in the $ABCB5^+$ population compared to the $ABCB5^-$ one. The data are supported by the reduction of these metastatic properties when ABCB5 is knowdown in MMICs. It is assumed that this role is due to an activation of the NF-κB pathway that subsequently exerts pro-tumorigenic effects. The activation of the NF-κB requires several molecules, *e.g.,* the p65 protein. It appears that ABCB5 promotes the stability of the p65 protein through the inhibition of its ubiquitination and degradation, contributing to the activation of the NF-κB pathway. Another study performed by Wilson *et al.* revealed an additional ABCB5-regulated signaling pathway in MMICs. They identified that ABCB5 controls the secretion of IL-1β that serves: (i) to maintain the undifferenciated phenotype of MMIC; (ii) to promote tumor growth through an IL-1β-IL8-CXCR1 cytokine signaling circuit [73].

Melanomagenesis results from either mutations activating an oncogene and inactivating a tumor suppressor or from mutations simultaneously inactivating two

tumor suppressors. Analyses of melanoma samples with mutations in ABCB5 show in 75% of cases additional mutations in *NRAS* (an oncogene) and in 62.5% of cases mutations in *CDKN2a* (a tumor suppressor gene), suggesting that *ABCB5* is a tumor suppressor. Sana *et al.* [78] recently carried out *in vitro* analyses to study the deleterious effect of mutations inactivating ABCB5 on the cell phenotype. The experiments were performed on the 17T and 63T human melanoma cells obtained from patients samples and which both carry activating mutation in the *NRAS* oncogene. In addition, the 63T cell line also harbors mutations in the *PTEN* and *CDKN2a* tumor suppressors. They have produced different clones from these two cell lines to stably overexpress either ABCB5 wild-type or ABCB5 with loss-of-function mutations. Afterwards, a series of tests were perfomed to assess: cell proliferation, anchorage independent growth, and migration abilities. The results have shown for the cells mutated for ABCB5 higher rate of proliferation, an increase in the number of colonies after the anchorage independent growth assay, and increased migration. Taken together, these data suggest that loss-of-function mutations in *ABCB5* accelerate the development of melanoma. To data, *in vivo* experiments on mice models are underway to transpose the results observed *in vitro* [78].

3.4 Characterization

Despite a strong body of evidence of a role of ABCB5 in cancer MDR, the transporter remains little characterized. Little is known about its subcellular localization, its substrates, and its physiological function. Moreover, its role in tumorigenesis remains controversial.

Gene knockout cell lines constitute a powerful strategy to study gene function through the loss-of-function phenotype. To date, three types of nucleases have been engineered to introduce site-specific DNA double-strand breaks (DSBs). In absence of a specific template donor, the cell repairs DNA by a mechanism of non-homologous end-joining DNA (NHEJ) repair. This mechanism leads to the apparition of small deletions or insertions (called indels) that frequently induce frameshift mutations and the apparition of premature stop codon. The zinc finger (ZF) and transcription activator-like effectors (TALEs) are the first nucleases developed. These proteins consist of DNA-binding domains that individually recognize either 3 (ZF) or 1 (TALEs) bp of DNA. The modulation and the assembling of several domains allow to target specific DNA sequences. Both ZF and TALEs can be coupled with the FokI nuclease that subsequently induce DSBs cleavage in DNA. These two strategies present some limitations, mainly due to their context-dependent specificity. In addition, the construction of TALEs complexes is time-consuming and costly [80].

The Clustered Regularly Interspaced Short Palindromic Repeats (CRISPR)/Cas9 has been developed more recently and is now widely used as powerful genome editing tool (**Figure 8**). The method is based on a complex formed by a guide RNA (gRNA) and a Cas9 endonuclease that can induce a double-strand break cleavage in a specific DNA region. The gRNA contains a RNA scaffold and a 20-nucleotide sequence complementary to the targeted loci. One of the few requirements of the gRNA is that the 3'-end of the targeted DNA region must directly be followed by a protospacer adjacent motif (PAM). It is essential for the binding of Cas9 to DNA. The PAM

sequence is specific to the Cas9 species, and the most commonly used in genome engineering is the *Streptococcus pyogenes (S. pyogenes)* Cas9 enzyme, which recognizes the 5'-NGG PAM motif. After DNA binding, Cas9 induces a double-strand break DNA cleavage three nucleotides upstream the PAM sequence, *i.e.* between the 17th and 18th nucleotide of the gRNA. Following the DNA cleavage, two scenarios may be considered. Firstly, in presence of a template donor, the cell repairs DNA by a mechanism of homology directed repair (HDR). The result consists of a gene correction or replacement depending on the template donor. Secondly, if non donor sequence is provided, the DNA cleavage is followed by a mechanism of NEJH DNA repair that leads to the deletion of several nucleotides, which in many case induces frameshift mutations [81, 82, 83].

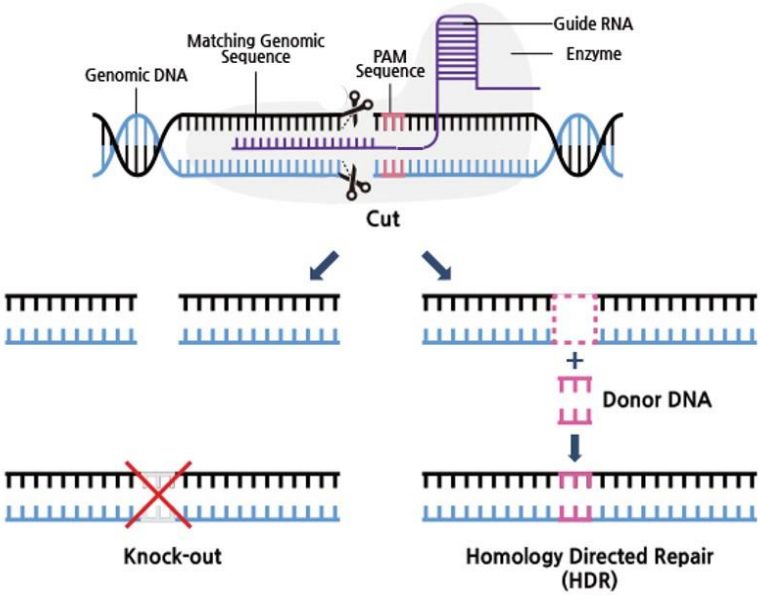

Figure 8: Overview of the CRISPR/Cas9 method. The guide RNA (gRNA) is composed of a scaffold and a 20-nucleotide sequence complementary to the targeted DNA region. The Cas9 enzyme is bound to the gRNA. The recruitment and binding of the gRNA/Cas9 complex to the targeted DNA region is directly followed by a protospacer-adjacent motif (PAM). The Cas9 endonuclease induces a double-strand break DNA cleavage. Two scenarios may be considered: (i) small nucleotide deletions resulting in frameshift mutations, (ii) a homology directed repair (HDR) in presence of a template donor, leading to gene replacement or correction. Figure adapted from Macrogen Humanizing Genome (available at: http://www.macrogen.com).

The CRISPR/Cas9 technique has several advantages over ZF and TALEs: unlike the ZF and TALEs strategies that recognize sequences by a protein-DNA interaction, the CRISPR/Cas9 directly targets genomic DNA regions with a specific gRNA. These gRNA are easily synthetized, highly specific, and they may be rapidly introduced inside the cell compared to the protein domains of both ZF and TALEs. Taking all these advantages, the CRISPR/Cas9 is now recognized as the most promising and powerful technique to induce genome modifications [84].

Objectives

The research project realized for this master thesis can be divided into two main parts. The first one is the creation of ABCB5-knockout human melanoma cell lines with the CRISPR/Cas9 tool. The second aims at better characterizing ABCB5 through the study of the transporter subcellular localization.

The generation of the ABCB5-knockout human melanoma cell lines will be performed on the Mel-Juso unpigmented primary melanoma cells with the CRISPR/Cas9 genome editing tool. The purpose is to remove a large fragment of the gene to prevent the expression of both the ABCB5 full-length and β isoforms. Three different RNA guides will be designed to target specific exons of the *ABCB5* gene in order to remove either a fragment of 53 kb or 125 kb. The proper deletion will be validated at the genomic level by screening PCR followed by sequencing, and the inhibition of protein synthesis will be assessed by Western Blot. In addition, the latter will prove and validate the specificity of the anti-ABCB5 antibodies used. The purpose of these ABCB5-knockout cell lines is to create a powerful tool to pursue the characterization of the ABCB5 transporter.

The study of ABCB5 subcellular localization will be performed by subcellular fractionation following the method described by de Duve *et al.* [85]. A first set of data from previous cell fractionation carried out by Sana *et al.* suggests a mixed localization of ABCB5 in the nuclear and microsomal fractions. However, these data have not been validated yet, mainly due to the lack of specificity of the antibodies used for the detection of ABCB5. If the ABCB5-knockout cell line confirms the specificity of these antibodies (*i.e.*, by the Western Blot mentioned above) a possible future work would be to perform a subcellular fractionation simultenaeously on both ABCB5-expressing and ABCB5-knockout Mel-Juso cell lines to get robust data about the transporter localization.

Materials and Methods

1. Choice of the model

1.1 Cell line and culture conditions

Human Mel-Juso unpigmented primary melanoma cells were used to generate the ABCB5 knockout (KO) cell line and to study the subcellular localization of the transporter. Cells were grown in Dulbecco's modified Eagle's medium (DMEM, Lonza, Belgium) supplemented with 10% heat-inactivated Fetal Bovine Serum (FBS, GE Healthcare Life Sciences, USA) and 0.1% of Pen/Strep (Gibco, Carlsbad, USA) under 5% CO_2 at 37°C.

1.2 ABCB5 constitutive expression

The constitutive expression of ABCB5 in ABCB5-expressing Mel-Juso cells was assessed and confirmed by reverse transcription followed by real-time PCR (RT-qPCR).

RNA extraction. Cells were first trypsinized and centrifuged at 1,200 rpm (Rottina 380 R, Hettich, Germany). 1 mL of Trizol (Fisher Scientific, Hampton, USA) was added and the cell lysate was conserved at -80°C. The following day, the lysate was thawed and 200 µL of chloroform was added (Fisher Scientific, Hampton, USA), before incubation for 5 min at room temperature (RT). Then, the tube was centrifuged at 12,000 g (Sigma 1-16K, Germany) for 15 min at 4°C, and the aqueous phase was recovered. Afterwards, the RNA was purified using the RNeasy Mini Kit of Qiagen (Hilden, Germany), following the instructions of the manufacturer. Finally, the RNA was quantified by spectrophotometry (Spectramax I3, Molecular Devices, Sunnyval, USA).

Reverse Transcription. cDNA's were synthesized from total RNA using the HighCapacity cDNA Reverse Transcription Kit (Thermo Fischer Scientific, Waltham, USA) and following the instructions of the manufacturer. The samples were conserved at 4°C before performing the qPCR.

Real Time PCR. The TaqMan qPCR reaction mixture was prepared in a total volume of 20 µL and contained: 10 µL of TaqMan Universal Master Mix (Thermo Fischer Scientific, USA), 1 µL of TaqMan probe (Life Technologies, Belgium), 8 µL of H_2O, and 1 µL of MelJuso cDNA. Different TaqMan probes were used to target four regions of the ABCB5 cDNA and one probe for the 18s cDNA. 18s was used as the housekeeping gene in the qPCR analyses as its expression is stable in Mel-Juso cell line. Samples were loaded on a 96-well plate (HardShellPCR plates 96-well, Bio-Rad laboratories, USA), and run on the qPCR machine (CFX96 Touch™ Real-Time PCR Detection System, Bio-Rad, USA). The thermal cycle conditions were as follows: 2 min at 50°C and 10 min at 95°C followed by 39 cycles at 95°C for 15 s and 60°C for 1 min. Results were then analysed with the CFX Manager™ Software (Bio-Rad, USA).

1.3 Transfection assay

Mel-Juso cells were transfected with TurboGFP plasmid (431 ng/mL), using either Lipofectamine 2000 (Invitrogen, Life Technologies, Belgium) or JetPrime™ (Polyplus transfection, France). The purpose was to assess and choose the most efficient method of transfection. The day before transfection, cells were seeded at a density of 25×10^3 cells/well in a 12-well plate and in 1 mL of complete growth medium (DMEM, 10% FBS, 0.1% Pen/Strep), to achieve 60-70% confluence the next day.

JetPrime. The mix for transfection was prepared following the protocol and the standard conditions (*i.e.*, 1:2 DNA to JetPrime ratio (w/v)) given by the manufacturer: TurboGFP plasmid (0.8 µg; 1.2 µg or 1.5 µg), JetPrime buffer, and JetPrime reagent. Then, 75 µL of the mix was added to each well and the plate incubated at 37°C for 48 h. Results were analyzed by flow cytometry (BD FACSVerse™, Biosciences, USA).

Lipofectamine 2000. The cell medium was removed 2 h before transfection and replaced by medium without Pen/Strep (DMEM, 10% FBS), at a volume of 500 μL per well. In one mix, the appropriate amount of DNA plasmid (1 µg; 1.6 µg; 2 µg or 2.5 µg) was diluted in 50 µL of Opti-MEM Reduced Serum Medium (Gibco, Life Technologies, Belgium). In a second mix, 50 µL of Lipofectamine 2000 Reagent were diluted in 250 µL of Opti-MEM Medium, and the mix was incubated for 20 min at RT. Then, 50 µL of diluted Lipofectamine 2000 Reagent were added to diluted DNA (1:1 ratio). The DNA-lipid complex was applied to the cells, and the plate incubated at 37°C for 48 h before analyzing the results by flow cytometry (BD FACSVerse™, Biosciences, USA).

Flow cytometry. After 48 h of incubation, cells were prepared for flow cytometry. The medium was removed and the cells were washed with 1 mL of PBS (DPBS, Lonza, Verviers, Belgium). Then, the cells were trypsinized with 200 µL of trypsin. 1 mL of medium (DMEM, 10% FBS, 0.1 % Pen/Strep) was added and the cell suspension transferred in a 15 mL tube. The tube was centrifuged at 300 g for 5 min (Rottina 380 R, Hettich, Germany) and the pellet was resuspended in 800 µL of PBS (DPBS, Lonza, Verviers, Belgium)/BSA (Carl Roth, Germany) 1%. The tube was centrifuged at 300 g for 5 min and finally resuspended in 400 µL of PBS/BSA 1%. Then, the cells were run on a BD FACSVerse™ flow cytometer (BD Biosciences, USA) and excited with the 488 nm laser line. 10,000 events were evaluated per sample. Analysis and calculation of the transfection efficiency were performed with the BD FACSuite software.

2. CRISPR/Cas9

2.1 Design of guide RNAs

Three guide RNAs (gRNAs) were designed to target exons 4 (150 bp), 15 (161 bp), and 27 (146 bp) of the full-length (FL) isoform of human *ABCB5* gene (NM001163941.1, NCBI Reference Sequence). The online-tool "Optimized CRISPR Design" from Zhang's laboratory (http://crispr.mit.edu) was used to determine and

classify the gRNAs available at the targeted loci and the best gRNAs were chosen to maximize on-target specificity (score (%)) and minimize the number of off-target sites (total off-targets and genic off-targets) (**Table 1**).

Name	Target	Sequence (5' - 3')	Total off-targets	Genic off-targets	Score (%)
4	Exon 4	GGACTAGACATCCACTAATA	74	2	86
15	Exon 15	GCAAAGGTCGGACTACAATCG	22	2	96
27	Exon 27	GTCATTATCGAGGGCTGAAG	85	3	82

Table 1: gRNAs designed to target specific exons in *ABCB5* by the CRISPR/Cas9 system.

2.2 Sequencing of ABCB5 targeted exons

Exons 4, 15, and 27 of the ABCB5 gene in Mel-Juso cell line were amplified by PCR and sequenced to assess the presence of single-nucleotide polymorphisms (SNPs) at the region targeted by the gRNA.

Genomic DNA extraction and quantification. DNA was extracted from Mel-Juso cell line. The culture medium (DMEM, 10% FBS, 0.1% Pen/Strep) was removed and cells washed with Dulbecco's Phosphate Buffered Saline (DPBS, Lonza, Verviers, Belgium). Cell suspension was centrifuged at 12,000 rpm for 10 min (Rottina 380 R, Hettich, Germany). The supernatant was removed and 200 µL of lysis buffer 1X (10 mM Tris-HCl pH 8, 50 mM KCl, and 0.1% Tween 20) added to the pellet. Tube was incubated at 95°C during 5 min, before adding 5 µL of proteinase K (Promega, Madison, WI, USA). The tube was incubated at 55°C for 30 min and afterwards centrifuged at 15,000 g for 2 min (Sigma 1-16K, Germany). The supernatant was recovered and 200 µL of isopropanol were added to precipitate DNA. Centrifugation was performed at 15,000 g for 2 min, before removing isopropanol. Then, 200 µL of ethanol 70% were added to the pellet. The tube was centrifuged at 15,000 g for 2 min, and the ethanol removed. The tube was dried for 15 min at RT. The pellet was suspended in 30 µL H_2O, before incubation at 65°C for 1 h, and under agitation. DNA was quantified using spectrophotometer (Spectramax I3, Molecular Devices, Sunnyval, USA). DNA was conserved at – 20°C before amplification by PCR.

DNA amplification. The PCR primers used are listed in **Table 2**. Each PCR reaction Mix was prepared in a final volume of 50 µL and contained: 25 µL of ready-to-use DreamTaq Green PCR Master Mix (2X) (ThermoFisher Scientific, Belgium), 5 µL of primer forward (10 µM), 5 µL of primer reverse (10 µM), 12.5 µL of H_2O, and 2.5 µL of DNA. PCRs were run using the following steps: initial denaturation step at 95°C for three min, and 35 cycles of 95°C denaturation temperature for 1 min, annealing temperature ranging from 56°C to 60°C depending on the primers for 1 min and 1 min of extension at 72°C followed by another 5 min of final extension at 72°C. PCR products were conserved at 4°C. PCR products were visualized in 1% agarose (Carl Roth, Germany) gel stained with ethidium bromide, after electrophoresis in a 1X TAE buffer at 100 V for 30 min. DNA ladder of 100 bp (Thermo Scientific, Belgium)

was used as size standard. Non-purified PCR products were sent for sequencing at Genewiz. Reverse PCR primers were used for the sequencing.

Target	Primer	Sequence (5' - 3')	Tm (°C)	Ta (°C)
Exon 4	F	TTTTACAGTTGTGGTGCTACG	64	59
	R	GCCTTGCTAGCTTAACGTTTGT	64	
Exon 15	F	GAGCAAAGGTCGGACTACAATC	66	60
	R	CTCTGAAACGTTAAACCCTGCT	64	
Exon 27	F	GCTTTCTTAATTGCATGCTCCT	62	56
	R27	ATTCTTTCCAGGCCTTTGTTTT	60	

Table 2: List of primers used for PCR amplification of ABCB5 gRNA/Cas9 targeted exons

2.3 Construction of the eSpCas9 plasmid

Each gRNA was cloned into an eSpCas9 plasmid from Feng Zhang's laboratory (#71814, Addgene, USA). The plasmid contains the *S. pyogenes* Cas9 enzyme under the control of the CBh promoter. The plasmid allows to clone each gRNA thanks to the presence of two BbsI restriction sites and allows to express these gRNAs by the U6 promoter. The oligonucleotides used for the cloning are listed in **Table 3**. Each of them was ordered with the gRNA sequence, a 5' end BbsI restriction enzyme site (*i.e.,* CACC for sense and AAAC for antisense oligos), and a phosphorylated 5' end to facilitate the ligation.

gRNA	Sense oligo (5'-3')	Antisense oligo (5'-3')
4	CACCGGACTAGACATCCACTAATA	AAACTATTAGTGGATGTCTAGTCC
15	CACCGCAAAGGTCGGACTACAATCG	AAACCGATTGTAGTCCGACCTTTGC
27	CACCGCTTCTCACTGTCATTATCGA	AAACTCGATAATGACAGTGAGAAGC

Table 3: Sequences of the oligonucleotides used for the cloning of gRNAs into the eSpCas9 plasmid.

Cloning. Oligonucleotides were annealed in a final volume of 10 μL containing: 1 µL of sense and 1 µL of antisense oligonucleotides (100 µM), and 8 µL of H_2O. The tube was heated at 95°C (Provocell™ Esco, Singapore) for 5 min and cold down at RT. Finally, annealed oligonucleotides were 200-fold diluted to obtain a final concentration of 0.5 µM.

The eSpCas9 plasmid was digested using the BbsI restriction enzyme (New England Biotechnologies, 10,000 U/mL). The mix for the digestion was prepared as follows: 10 µg of eSpCas9 plasmid, 10 µL of CutSmart Buffer 10X (New England Biotechnologies), 5 µL of BbsI restriction enzyme (New England Biotechnologies, 10,000 U/mL) and the corresponding volume of nuclease-free water to achieve a final volume of 100 µL. The mix was incubated at 37°C for 1 h (Provocell™ Esco,

Singapore) before inactivating the BbsI enzyme at 65°C for 20 min. The verification of the plasmid digestion was assessed by electrophoresis on an agarose gel 1% with ethidium bromide (Carl Roth, Karlsruhe, Germany). Non-digested eSpCas9 plasmid was used as control. Both digested and non-digested plasmids were mixed with 6-fold diluted loading blue buffer (0,2% Bromophenol blue (p/v), 0,2% xylene cyanole (p/v), 30% glycerol (v/v) in Tris-EDTA, 6-fold concentrated). Then, the migration was performed at 120 V for 25 min before visualization using the Gel Doc XR$^+$ System (BioRad, USA).

The eSpCas9 plasmid was dephosphorylated at the 5' end to prevent the formation of empty plasmid during the step of ligation. The dephosphorylation was performed by the addition of 4 µL of the rSAP phosphatase (New England BioLabs, USA) into the product of digested plasmid. The mix was incubated at 37°C before inactivating the enzyme at 65°C for 5 min.

Each pair of annealed oligonucleotides (0.5 µM) was cloned into a digested and dephosphorylated eSpCas9 plasmid. The ligation was performed in a final volume of 20 µL containing: 1 µL of digested plasmid (100 ng/µL), 2 µL of annealed oligos (0.5 µM), 1 µL of T4 DNA ligase (New England Biolabs, USA), 2 µL of T4 DNA ligase Buffer (New England Biolabs, USA), and 14 µL of H_2O. One condition without any pair of oligonucleotides was employed as negative control. The ligation was performed overnight at 16°C and then the products of ligation were conserved at -20°C before amplification in *E. Coli*.

Amplification. The eSpCas9 plasmids were amplified using the bacterial system *E. Coli* DH5*α*. The first day, four transformations were performed: three with the eSpCas9 plasmid ligated to a pair of annealed oligonucleotides and one empty plasmid as negative control. For each condition, 20 ng of plasmid were added to 50 µL of competent bacteria. The transformations were carried out by heat shock: 30 min on ice, 45 s at 42°C (Provocell^{TM} Esco, Singapore) followed by 10 min on ice. Afterwards, 700 µL of LB (Carl Roth, Karlsruhe, Germany) were added to the mix and the tube was incubated at 37°C for 1 h and under 210 rpm shaking (Provocell^{TM} Esco, Singapore). Then, bacteria were spread on LB (Carl Roth, Karlsruhe, Germany)/ampicillin (Sigma-Aldrich, Saint-Louis, USA) agar plates and incubated at 37°C overnight. The following day, ten colonies were isolated for each condition.

The proper ligation of the oligonucleotides into the eSpCas9 plasmid was assessed by PCR. PCR primers were chosen in such a way that the amplification is positive only if the ligation occured. Reverse primer (5' TACCGTAAGTTATGTAACGGG) was common for all conditions and complementary to a region within the eSpCas9 plasmid. Forward primer was specific of the condition and corresponded to the antisense of the ligated oligonucleotide (**Table 3**). The PCR mix was prepared as follows in a final volume of 20 µL: 10 µL of DreamTaq Green PCR 2X Master Mix (Thermo Fischer Scientific, Waltham, USA), 2 µL of reverse primer (10 µM), 2 µL of forward primer (10 µM), 100 ng of plasmid, and the corresponding volume of H_2O. PCR amplification of 35 cycles (C1000 touch thermal cycler, BioRad, Hercules, USA) was programmed with a DNA denaturation for 1 min at 95°C, primers hybridization during 1 min at 59°C (*i.e.*, annealing temperature, similar for all conditions), and polymerisation by the polymerase at 72°C for 3 min. Then, PCR products were visualized on an agarose gel

1% with ethidium bromide (Carl Roth, Karlsruhe, Germany) after a migration at 120 V for 25 min. For each condition, two positive colonies were selected for the further amplification step.

The selected colonies were placed in 2.5 mL of LB (Carl Roth, Karlsruhe, Germany)/ ampicillin (Sigma-Aldrich, Saint-Louis, USA). Amplification was performed overnight at 37°C and under 210 rpm shaking (New Brunswick Innova 4000).

Purification. The next day, plasmids were purified using the kit PureYield™ Plasmid MiniPrep System (Promega, Madison, USA) and following the instructions given by the manufacturer. Expression plasmids were quantified using a spectrophotometer (Spectramax I3, Molecular Devices, Sunnyval, USA) and stored at -20°C until utilization for cell transfection.

2.4 Transfection

Mel-Juso cells were transfected with three plasmids: two eSpCas9 plasmids cloned with the gRNAs of the tested conditions and one pTRIPZ plasmid containing the puromycin gene resistance, to serve as selection marker of transfected cells.

The day before transfection, cells were seeded at a density of 25 $\times 10^3$ cells/well in a 12-well plate and in 1 mL of complete growth medium (DMEM, 10% FBS, 0.1% Pen/Strep), to achieve 60-70% confluence the next day. Cells were transfected using JetPrime™ (Polyplus transfection, France) reagent. The mix for transfection was prepared following the protocol and the standard conditions (*i.e.*, 1:2 DNA to JetPrime ratio (w/v)) given by the manufacturer: 1 µg of the eSpCas9 and pTRIPZ plasmids mix, JetPrime buffer, and JetPrime reagent. Then, 75 µL of the mix was added to each well and the plate was incubated at 37°C for 24 h. Afterwards, the medium was changed and 2 µg/mL of puromycin (10 mg/mL, Gibco Life Technologies, China) were added for 24 h to select cells resistant to the antibiotic (*i.e.,* cells having incorporated the pTRIPZ plasmid).

2.5 Generation of monoclonal cell populations

The generation of monoclonal cell populations positive for either the deletion 53 kb or 125 kb in *ABCB5* was performed by seeding transfected cells in 96-well plates at a density of one cell per well.

Following cell counting (Vi-Cell XR Analyzer, Life Sciences, IN, USA) three different solutions were prepared with respectively 30, 50, or 60 cells in a final volume of 20 mL growth medium (DMEM, 10% FBS, 0.1 % Pen/Strep). Then, 200 µL from each solution were placed per well in 96-well plates to seed on average a density of one cell per well. When cell confluence reached 100%, cells were harvested. Two-third of the cell suspension were used for genomic DNA extraction and screening PCR. The rest of cell suspension was conserved at -80°C after addition of cell freezing medium (70% DMEM, 20% DMSO, 10% FBS, 0.1 % Pen/Strep).

2.6 Knockout validation by PCR screening

DNA extraction. The culture medium (DMEM, 10% FBS, 0.1% Pen/Strep) was removed and cells washed with Dulbecco's Phosphate Buffered Saline (DPBS, Lonza, Verviers, Belgium). Cell suspension was centrifuged at 1,200 rpm for 10 min (Rottina 380 R, Hettich, Germany). The supernatant was removed and 200 µL of lysis buffer 1X (10 mM Tris-HCl pH 8, 50 mM KCl, and 0.1% Tween 20) added to the pellet. Tube was incubated at 95˚C during 5 min, before adding 5 µL of proteinase K (Promega, Madison, WI, USA). The tube was incubated at 55˚C for 30 min and afterwards centrifuged at 15,000 g for 2 min (Sigma 1-16K, Germany). The supernatant was recovered and 200 µL of isopropanol were added to precipitate DNA. Centrifugation was performed at 15,000 g for 2 min, before removing isopropanol. Then, 200 µL of ethanol 70% were added to the pellet. The tube was centrifuged at 15,000 g for 2 min, and ethanol removed. The tube was dried for 15 min at RT. The pellet was suspended in 30 µL H_2O before incubation at 65˚C for 1 h, and under agitation. DNA was quantified using spectrophotometer (Spectramax I3, Molecular Devices, Sunnyval, USA). DNA was conserved at – 20˚C before screening PCR.

PCR amplification. After DNA extraction, different PCR were carried for each condition: the exons targeted by the gRNAs were individually amplified and an additional PCR was performed to determine if the 53 kb or 125 kb fragment was removed. The PCR primers used are listed in **Table 4** and the different PCR performed in **Table 5**. PCR were run using the following protocol: initial denaturation at 95˚C for 3 min, and 35 cycles of 95˚C denaturation temperature for 1 min, annealing temperature depending on the primers (ranging from 53˚C to 59˚C) for 1 min, and 1 min of extension at 72˚C followed by another 5 min of final extension at 72˚C. PCR products were conserved at 4˚C before visualization in 1% agarose (Carl Roth, Germany) gel stained with ethidium bromide, after electrophoresis in a 1X TAE buffer at 120 V for 30 min. DNA ladder of 100 bp (Thermo Scientific, Belgium) was used as size standard.

Target	Primer	Sequence (5' - 3')	Tm (˚C)
Exon 4	F4	TTTTACAGTTGTGGTGCTACG	64
	R4	GCCTTGCTAGCTTAACGTTTGT	64
Exon 15	F15	TCTTAAACATGCAAAGGTTGTT	57.4
	R15	AACGTTAAACCCTGCTGACA	59.7
Exon 27	F27	GCTTTCTTAATTGCATGCTCCT	62
	R27	ATTCTTTCCAGGCCTTTGTTTT	60

Table 4: List of primers used for the screening PCR

Amplification	Primers	Ta (°C)	Product size (bp)
Exon 4	F4 & R4	59	270
Exon 15	F15 & R15	53	275
Exon 27	F27 & R27	56	280
53 kb deletion (4 and 15)	F4 & R15	54.7	318
125 kb deletion (4 and 27)	F4 & R27	59	230

Table 5: PCRs screening to amplify targeted exons and to detect the deletions.

3. Subcellular fractionation

3.1 de Duve's fractionation

Two days before performing the subcellular fractionation, Mel-Juso cells were seeded in 10 petris dishes completed with 7 mL growth medium (DMEM, 10% FBS, 0.1% Pen/Strep) to achieve 80% confluence the next day. All steps of fractionation were performed on ice. First, cells were washed four times with 4 mL of 0.25 M cold sucrose solution. Then, cells of each dish were detached and pooled in a Dounce homogenizer in a final volume of 2 mL sucrose solution. Cells were disrupted with six strokes of the pestle and the cell homogenate was centrifuged at 1,000 g (Allegra, Beckman Coulter, USA) for 9 min 16 sat 4°C. The supernatant (E1) was decanted and kept on ice. The pellet (N) was resuspended and rehomogenized in the Dounce by six strokes with the pestle. Afterwards, N was transferred in a tared 15 mL tube and made up to a final volume of 2 mL sucrose solution, before centrifugation at 1,000 g (Allegra, Beckman Coulter, USA) for 7 min 32 s at 4°C. The supernatant (E2) was collected and combined with E1, both representing the cytoplasmic extract (E). The pellet N was resuspended in a final volume of 1 mL sucrose solution, weighted, and kept on ice. One aliquot of the cytoplasmic extract E was removed and kept on ice for further analysis. Then, the rest of the fraction was further fractionated in a L7-35 ultracentrifuge (Beckman Coulter, USA) using the TI 50 Rotor. Three particular fractions (two mitochondrial (M and L) and one microsomal (P)) were successively isolated by sequentially increasing speed of centrifugation. Firstly, E was centrifuged at 8,000 rpm at 4°C for 2 min 24 s. The supernatant (LPS1) was collected and transferred into a tared tube of 15 mL. The pellet (M) was resuspended and made up to a final volume of 2 mL sucrose solution. Then, the fraction was centrifuged at 8,000 rpm at 4°C for 2 min 24 s. The supernatant (LPS2) was collected and combined with LPS1 to form LPS. M was resuspended in a final volume of 500 µL sucrose solution, weight, and kept on ice. The LPS supernatant was centrifuged at 25,000 rpm for 2 min 24 s at 4°C. The supernatant (PS1) was collected and transferred into a tared tube of 15 mL. The pellet (L) was resuspended and made up in a final volume of 2 mL sucrose solution, before centrifugation at 25,000 rpm at 4°C for 2 min 52 s to wash the fraction. The supernatant (PS2) was collected and combined with PS1 to form PS. The pellet L was resuspended in a final volume of 500 µL sucrose solution, weighted, and kept on ice. Finally, PS was centrifuged at 35,000 rpm for 35 min at 4°C. The supernatant (S) was collected and transferred into a tared 15 mL tube. 1 mL was sampled for future

analyses and the rest was thrown. P was resuspended in 500 µL sucrose solution, weight, and kept on ice. For each fraction, primary dilutions were calculated by dividing the volume of the fraction by the amount of starting material.

After fractionation, six fractions were collected (E, N, M, L, P, and S). The amount of proteins in each of them was determined with the Bradford protein assay (BioRad Laboratories, USA) and following the instructions given by the manufacturer.

3.2 Enzymatic dosages

The activity of five enzymes markers was measured: *β*-galactosidase (lysosome), alkaline *α*-glucosidase (endoplasmic reticulum), alkaline phosphodiesterase (plasma membrane), dipeptidyl peptidase 3 (cytosol), and cytochrome C oxidase (mitochondria).

B-galactosidase. The activity of *β*-galactosidase was assessed by fluorimetry (BioRad, USA). The reaction was performed in duplicate for each fraction. The mix for each reaction was prepared in a final volume of 190 µL containing: 2.5 µL of 40 mM 4-MU*β*-galactopyranoside substrate (Sigma-Aldrich, Germany), 25 µL of NaCl 0.4 M, 50 µL of acetate buffer 0.2 M pH 5, 112 µL H_2O, and 0.5 µL of Triton X-100 20% (Promega, USA). Then 5 µL and 10 µL of each fraction were added in two cuvettes, before incubation at 37°C in a water-bath for 45 min. Afterwards, the reaction was stopped by adding 1.2 mL of glycine-NaOH buffer (50 mM, EDTA (Carl Roth, Germany) 5 mM, 0.05% Triton, pH 10.5), before reading fluorescence emission at 450 nm.

Alkaline *α*-glucosidase. The activity of the enzyme was assessed by fluorimetry (BioRad, USA). The test was performed in duplicate for each fraction. First, 0.676 mg of 4-MU*α*-D-glucopyranoside (Carl Roth, Belgium) substrate were dissolved in 200 µL of ethanol 50%, at 37°C. Then, the mix for the reactions was prepared in a final volume of 1.5 mL containing: 300 µL of glycine-NaOH buffer (0.5 M, pH 9), 3 µL of Triton X-100 20% (Promega, USA), 150 µL of substrate, and 1.05 mL of H_2O. Afterwards, 90 µL of the mix were added in each cuvette, and 5 µL or 10 µL of the corresponding fraction were added, before incubation in a water-bath at 37°C for 1 h. The reaction was stopped by adding 1 mL of glycine-NaOH buffer (0.1 M, pH 10.4) before reading fluorescence emission at 450 nm.

Alkaline phosphodiesterase. The enzymatic activity was assessed by colorimetry. The reaction was performed in duplicate for each fraction. First, the mix for all reactions was prepared with: 1.75 mg of thymidine 5'-monophosphate p-nitrophenyl ester sodium salt substrate (Sigma-Aldrich, Germany), 507 µL of glycine hydroxide buffer (0.5 M, pH 9.6), 507 µL of zinc acetate 0.01 M, 30.43 µL of NaOH 1M, and 1.22 mL of H_2O. Then, 115 µL of the mix were added in each cuvette and 5 µL or 10 µL of the corresponding fraction were added. The reaction was incubated in a water-bath at 37°C and for 3 hours. The reaction was stopped by adding 1 mL NaOH 0.1 M before reading absorbance at 400 nm with a spectrophotometer Lambda 10 (PerkinElmer, USA).

Dipeptidyl peptidase 3. The activity of the enzyme was measured by fluorimetry (BioRad, USA). The reaction was performed in duplicate for each fraction. The mix for the reactions was prepared with: 500 µL of Tris-Cl buffer (0.5 M, pH 8), 19.97 µL of H-Arg-Arg-7-amido-4-methylcoumarin hydrochloride substrate (25 mM), and 950.5 µL of H_2O. Then, 90 µL of the mix were placed in each cuvette and 5 µL or 10 µL of the corresponding fraction were added. The reaction was incubated in a water-bath at 37°C for 1 hour. Then, the reaction was stopped by adding 1.2 mL glycine (50 mM, EDTA (Carl Roth, Germany) 5 mM, Triton X-100 0.05%, pH 10.5), before reading the fluorescence emission at 460 nm.

Cytochrome C oxidase. The activity of the cytochrome C oxidase was assessed by colorimetry. The methods consists in following the decrease of absorbance at 550 nm of reduced cytochrome C due to its oxidation by the cytochrome C oxidase. The solutions required for the assay were prepared as describe below. One dilution solution in a final volume of 100 mL with: 2 mL of Triton X-100 2%, 1 mL EDTA (Carl Roth, Germany) (0.1 M, pH 7.4), 0.2 mL of phosphate buffer (0.5 M, pH 7.4), and H_2O. Each fraction was two-fold diluted in this solution before performing the assay. One mix with the substrate was made in a final volume of 25 mL with: 6.55 mg of cytochrome C substrate (SigmaAldrich, USA), 1.45 mL of phosphate buffer (0.5 M, pH 7.4), 242.6 µL of EDTA (Carl Roth, USA) (0.1 M, pH 7.4), and H_2O. The enzymatic reaction was performed for each fraction in a cuvette containing 1 mL of mix substrate and 50 µL of the corresponding two-fold diluted fraction. One cuvette was prepared to obtain 100% reduced cytochrome C, by adding potassium ferricyanide (Science Company, USA) to 1 mL of the substrate mix. One cuvette was prepared to obtain 100% of oxidized cytochrome C, by adding dithionite to 1 mL of the substrate mix. Then, the analysis was performed by spectrophotometry and with the UV WinLab Software (PerkinElmer, USA), following the protocol given by the manufacturer.

3.3 Western Blot

Western Blot was performed to obtain the distribution profiles of histone H1 (marker of the nucleus) and ABCB5. First, 15 μg of each fraction were denaturated at 37 °C for 30 min in 45 µL of loading buffer. The proteins were then loaded in either an 8% (ABCB5) or 15% (histone H1) SDS acrylamide gel and migration was performed at 110 V for 1h45. Then proteins were blotted to a PVDF membrane (BioRad, USA) at 110 V during 2 h. After blocking the membrane 30 min in a 3% milk PBS 0.1% Tween 20 solution, the anti-histone H1 (monoclonal mouse (ThermoScientific)) and the anti-ABCB5 (polyclonal goat (Rockland, 600-401-A77S)) antibodies were 500-fold diluted in PBS 0.1% Tween 20 3% milk and incubated with the membrane overnight. The followig day, the membranes were washed four times during 5 min in PBS 0.1 % Tween 20 before incubation with the appropriate secondary antibody (anti-mouse or anti-goat) in a 3000-fold diluted solution of PBS 0.1% and Tween 20 3% milk. After four final washing of 5 min with PBS 0.1% Tween 20, the membranes were revealed with the Western Lightning Plus-ECL kit (PerkinElmer, Waltham, USA). The bands at the expected protein size for histone H1 were quantified using the ImageJ software and the distribution profile of the protein was graphically represented.

Results and Discussion

1. Characterization of Mel-Juso cell line

1.1 ABCB5 constitutive expression

We performed a real-time PCR on the parental Mel-Juso cell line to assess the constitutive expression of ABCB5. The four TaqMan probes were chosen to hybridize different regions of the *ABCB5* gene (**Figure 9**): the probes 40 and 51 target sequences found both in the ABCB5 full-length (FL) and *β* isoforms and the probes 39 and 41 only recognize regions of the ABCB5FL isoform.

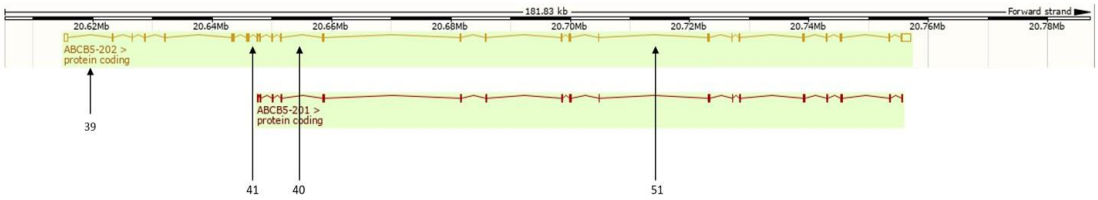

Figure 9: TaqMan probes hybridization sites on the *ABCB5* gene. Top: representation of the ABCB5 full-length (FL) isoform; bottom: representation of the ABCB5*β* isoform. Probes 40 and 51 recognize common regions of both the ABCB5FL and *β* isoforms. Probes 39 and 41 only target sites of the ABCB5FL.

The results are shown in **Figure 10**. Each condition was performed in triplicate and the 18S ribosomal RNA was used as positive control. The mean Ct values for the different probes targeting ABCB5 are: 39.73 (ABCB5 39), 25.29 (ABCB5 40), 36.50 (ABCB5 41), and 26.77 (ABCB5 51). The data show lower Ct values for the probes targeting both the full-length and *β* isoforms (*i.e.*, 40 and 51) compared to those only hybridizing the ABCB5 full length (*i.e.*, 39 and 41). It indicates that Mel-Juso cells at least express the *β* isoform. However, the real-time PCR does not allow to conclude if the cell line also expresses the full-length isoform. The mean Ct values for probes 39 and 41 are higher than 30, and beyond this value, results are often considered as false positive that may result: either from primers dimers formation or from a non-specific amplification. Although other techniques exist to detect and analyze the abundance of specific mRNA (*e.g.*, Nothern Blot, nuclease protection assays, *in situ* hybridization, etc.), the real-time PCR remains the most sensitive method. It is likely that the Mel-Juso cells do not express the full-length isoform at all.

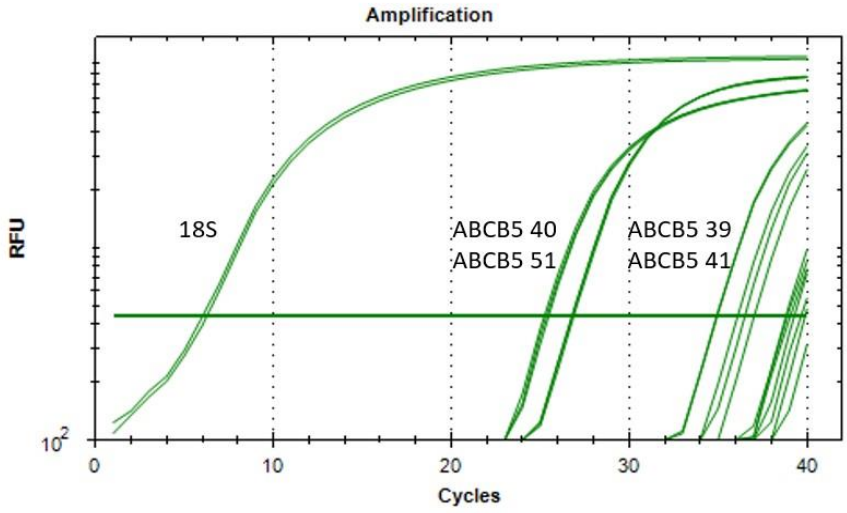

Figure 10: Analysis of ABCB5 constitutive expression in Mel-Juso parental cells. The relative fluorescence unit (RFU) is plotted against cycle. The threshold (horizontal line) is set. The five TaqMan probes chosen target: 18S ribosomal RNA (positive control), both ABCB5 full-length and β isoforms (ABCB5 40 and 51), or only the full-length isoform (ABCB5 39 and 41). The experiment was performed in triplicate and the mean Ct values were calculated for each condition. Amplifications run with the BD FACSVerse flow cytometer and analyses performed with the BD FACSuite software.

1.2 Transfection

JetPrime and Lipofectamine 2000 reagents were used to transfect the TurboGFP plasmid in parental Mel-Juso cells. The purpose was to determine the most efficient method of transfection for the future transfections with the CRISPR/Cas9 system. The GFP emission was detected 48 h post-transfection by fluorescence activating cell sorting (FACS) and the results were analyzed by the BD FACSuite software (**Figure 11**).

Non-transfected Mel-Juso cells (**11(a)**) were used to define the thresholds of forward scatter (FSC) and side scatter (SSC) parameters to gate cells (P1, orange), and to determine the background fluorescence to subtract during the analysis of GFP emission by transfected cells (purple). The transfection efficiency (*i.e.*, the percentage of cells transfected) was calculated for each condition depending on the transfection reagent and the amount of TurboGFP plasmid transfected.

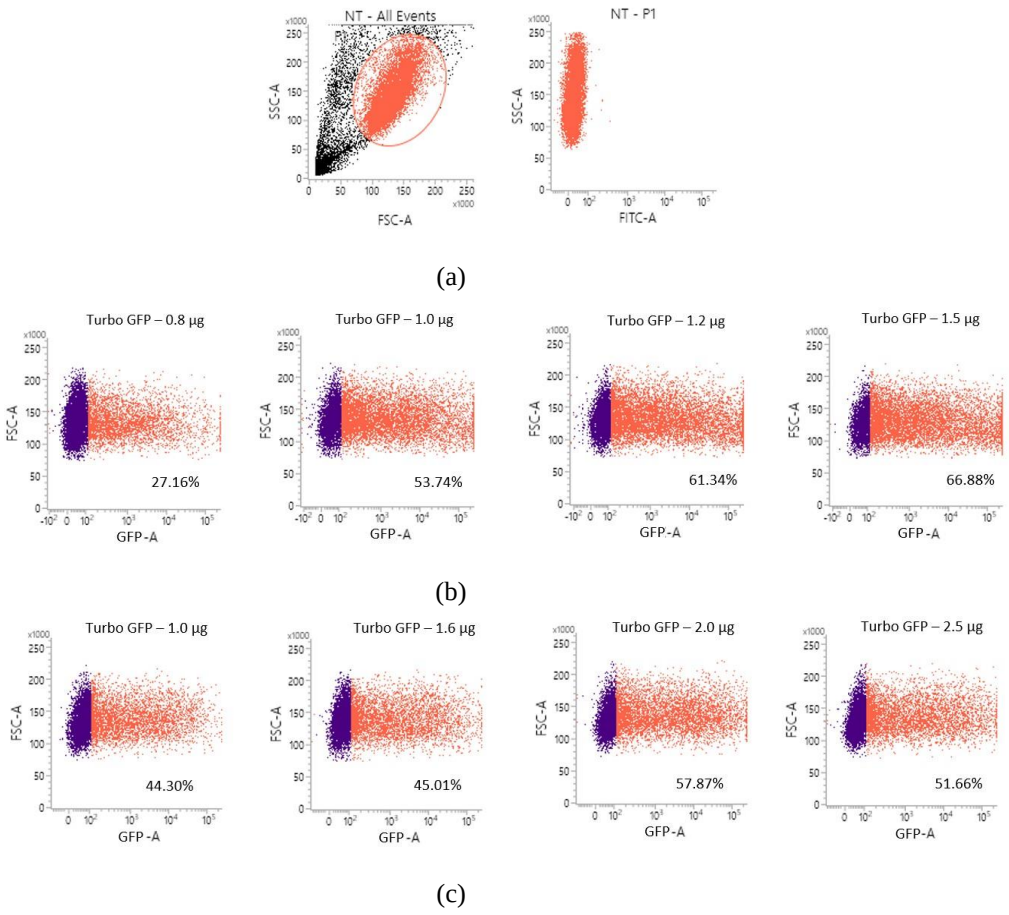

Figure 11: Detection of GFP emission in Mel-Juso parental cells by flow cytometry analysis. (a) Non-transfected Mel-Juso (NT) cells used: (i) to set up forward scatter (FSC) and side scatter (SSC) parameters to gate cells (P1, orange) (left panel) and (ii) to determine the background fluorescence (right panel) to subtract during analysis of GFP emission by transfected cells. (b) Transfection of Mel-Juso cells with JetPrime reagent and different amounts of TurboGFP plasmid (0.8 µg; 1.0 µg; 1.2 µg; 1.5 µg). X-axis: intensity of GFP emission (GFP-A). Background fluorescence (purple) removed from the analysis; y-axis: cell size (FSC-A). Analysis performed on gated population (P1, orange). The transfection efficiency (%) was measured for each condition by the BD FACSuite software. (c) Transfection of Mel-Juso cells with Lipofectamine 2000 reagent and different amounts of Turbo-GFP plasmid (1.0 µg; 1.6 µg; 2.0 µg; 2.5 µg). X-axis: intensity of GFP emission (GFP-A). Background fluorescence (purple) removed from the analysis; y-axis: cell size (FSC-A). Analysis performed on gated population (P1, orange). The transfection efficiency (%) was measured for each condition by the BD FACSuite software.

The results show that the percentage of transfection is on average 52.28% with JetPrime reagent (**11(b)**) and 49.71% with Lipofectamine 2000 (**11(c)**), indicating that both transfection reagents successfully transfect the Mel-Juso cell line. However, it is likely that the calculated mean value for JetPrime is underestimated. The low percentage (27.16%) of transfection obtained with 0.8 µg of TurboGFP plasmid is not consistent with the three other values obtained (higher than 50%). We hypothetize that a higher cell confluence in this specific condition before transfection had led to an important decrease of the transfection efficiency. However, we should at least performed each condition in duplicate to compare the results.

From these results, we chose the JetPrime reagent for the future transfections with the CRISPR/Cas9 system since (i) the reagent has already been successfully used in different CRISPR/Cas9 applications, and (ii) because JetPrime presents many

advantages over other methods. For instance, the technique requires low amount of foreign DNA and transfection reagent to achieve high transfection efficiency. Our data support this statement (*e.g.,* an efficiency of 66.88% is achieved after transfection of 1.5 µg of TurboGFP). Other studies have analyzed on different cell lines, the percentage of GFP-positive cells after transfection either with JetPrime or Lipofectamine 2000 (**Figure 12**). For JetPrime, they used half of the amount of reagent and transfected DNA compared to Lipofectamine 2000. The results show that even with a lower amount of reagent and DNA, the transfection efficiency is always higher with JetPrime, and over than 70% [86, 87].

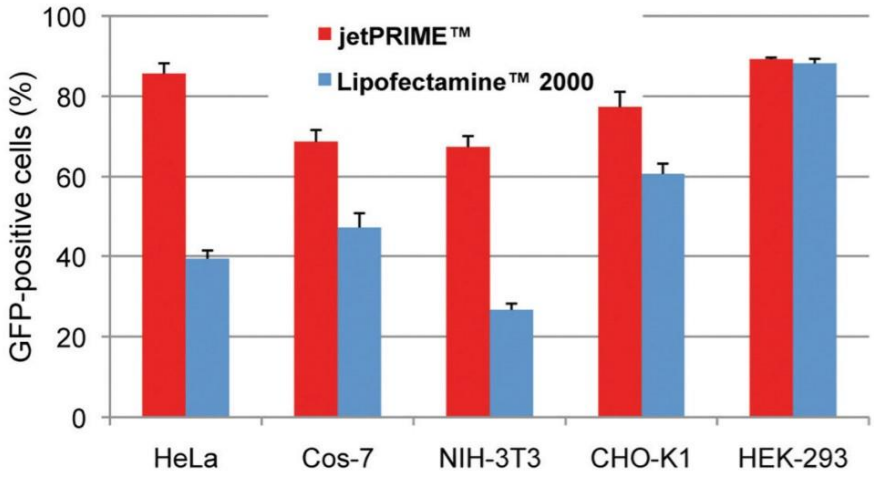

Figure 12: Percentage of GFP-positive cells after transfection either with JetPrime or Lipofectamine 2000. The transfection with JetPrime was performed with half of the amount of transfected DNA and reagent compared to Lipofectamine 2000. In all cases the percentage of GFP-positive cells (*i.e.*, the transfection efficiency) is higher with JetPrime and over 70%. Figure adapted from Polypus.

Moreover, JetPrime is particularly suitable for multiple plasmids co-transfection [88]. This property is important for our future experiments as we will transfect a panel of three plasmids in each tested condition (two eSpCas9 plasmids cloned with a specific gRNA and one pTRIPZ plasmid for the selection of transfected cells).

Finally, JetPrime shows lower cytotoxic effects than Lipofectamine 2000 and results in higher cell viability. The delivery of the JetPrime complex to the cell is gentle and respects the cell morphology. It is due to the nature of the JetPrime reagent, a cationic polymer-based molecule which forms positively charged complexes with plasmid DNA. Unlike cationic lipids such as Lipofectamine 2000, the JetPrime complex does not destabilize the cell membrane and is captured by the cell *via* the endolysosomal pathway. It is followed by a proton-spong effect that leads to the release of plasmid DNA in the cytosol. The proton sponge effect is due to the polymeric nature of the JetPrime reagent, which attracts H^+ within the lysosome. The decrease of the intra-lysosomal pH is compensated by an influx of both Cl^- and water, which finally leads to the swelling and the disruption of the organelle, and the release of DNA [88].

2. CRISPR/Cas9: optimization

2.1 Design of the gRNAs

We firstly defined the regions to target in the *ABCB5* gene. The real-time PCR shows that Mel-Juso parental cells at least express the ABCB5 transporter under the *β* isoform, but the results do not allow us to conclude if the cells also express the ABCB5 full-length isoform. Because the purpose of this project is to generate an ABCB5-knockout cell line for all isoforms, the best way would be to completely remove the gene, *i.e.,* a fragment of 150 kb. In this case, both the mRNA transcription and the protein expression would be knock-down. However, it appears that, in mammalian cells, the larger is the size of the fragment to remove, the lower is the efficiency of the CRISPR/Cas9 tool [89].

We have decided to test two conditions: the first one is to remove a fragment of 125 kb and the second one is to remove a fragment of 53 kb in the *ABCB5* gene. For that purpose, we have selected three exons to target *ABCB5*: exons 4, 15, and 27. The choice of exons 4 and 15 is based on the beginning of the coding regions of either the ABCB5 full-length or the *β* isoform, respectively. Depending on the condition, Mel-Juso cells will be co-transfected with two gRNAs targeting either exons 4 and 15 (to remove 53 kb) or exons 4 and 27 (to remove 125 kb). In both conditions, we expect to inhibit the ABCB5 protein synthesis. However, it is likely that only the 125 kb deletion will also prevent the mRNA transcription.

We designed and selected three gRNAs with the "Optimized CRISPR Design" software from Zhang's laboratory (available at: http://crispr.mit.edu/) (**Table 6**). The choice of the gRNAs was based on three important criteria: the number of total off-targets, the number of genic off-targets, and a specificity score. The number of total off-targets consists of possible hybridization of the gRNA with another coding or non-coding genomic sequence. The number of genic off-targets is more precise and represents the binding of the gRNA followed by the Cas9 cleavage in other exons than the targeted one. Finally, the software provides a score corresponding to the specificity of the gRNA for its target and is quality indicator of the gRNA [90]. The number of genic off-targets is one of the most important criteria and this number needs to be as low as possible. Indeed, gene disruption can have consequences on its transcription, on protein production, and can modify the cell phenotype. We observe that all gRNAs show maximum three genic off-targets, which is considered as very low.

Name	**Target**	**Sequence (5' - 3')**	**Total off-targets**	**Genic off-targets**	**Score (%)**
4	Exon 4	GGACTAGACATCCACTAATA	74	2	86
15	Exon 15	GCAAAGGTCGGACTACAATCG	22	2	96
27	Exon 27	GTCATTATCGAGGGCTGAAG	85	3	82

Table 6: gRNAs designed to target specific exons in *ABCB5* by the CRISPR/Cas9 system.

2.2 Genic off-targets analysis

We performed further analysis of these potential genic off-targets with the "Optimized CRISPR design" software to identify: the sequence of the off-target, the chromosome location, the number of mismatches between the sequence of the off-target and the gRNA, and a score depending on mismatch tolerance. The latter mainly depends on two criteria: the mismatches localized between the 8^{th} and the 14^{th} nucleotide at the 3' end of the gRNA are less tolerated than those present at the 5' end; more than three mismatches are not tolerated and usually inhibit the off-target effect. The results show for all potential genic off-targets a number of mismatches higher than three and a very low tolerance score, meaning that the mismatches present in the off-target sequences are not well tolerated by the gRNA (**Table 7**). Thereby, the probability of gRNA hybridization and mutagenesis seems very low. However, it is important to be aware of the existence of these off-targets, *e.g.*, for future studies of the *ABCB5* gene function in which changes in the cell phenotype are expected. In this specific case, off-target effects may be a source of bias and may interfere with the results.

gRNA	Genic off-target sequence (5' - 3')	Site	Mismatches number	Score
4	GGAATAGAAATCCAATAAAA	chr. 12	4 [4:9:15:19]	0.1
	GGAATAGAAATGCTCTAATA	chr. 6	4 [4:9:12:14]	0.1
15	CAAAGGTCAGCCCACAATCA	chr. 3	4 [9:11:13:20]	0.1
	CAAAGGTCAGCCTTCAATCC	chr. 15	4 [9:11:14:20]	0.0
27	GACATTTTCCAGAGCTGAAG	chr. 16	4 [2:7:10:13]	0.4
	GGCATTATGGAGGGCTGGAA	chr. 15	4 [2:9:18:20]	0.1
	GTCAGTACCGAGACCTGAAG	chr. 4	4 [5:8:13:14]	0.1

Table 7: Analysis of the potential genic off-targets

We identified and analyzed the function of the seven genes found within these off-targets regions (**Table 7**). Most of them (*STYK1*, *ORC3*, *KNL1*, *RHOV*, and *EGF*) work as regulators of cell division, proliferation, and differentiation. *GPDL1* has an independent role specific to cardiac cells. Consequently, the gene is probably not expressed by melanoma cells. Finally, the function of *VATL1* is unclear and there is currently no validated data about it. Identifying the function of the proteins coded by these off-targets genes provides first insights about potential modifications that we could observe in the cell phenotype. We speculate that if mutation occurs in one of these genes, consequences could be, *e.g.*, a slow-down in cell proliferation, a decrease in cell viability, or a modification of cell morphology. Although the probability of off-target mutagenesis seems low, it would be relevant to sequence these seven genomic DNA regions to assess and confirm that the genes are not mutated. This kind of analysis is particularly important before performing functional studies on the *ABCB5* gene, as off-target effects may confound the interpretation of biological phenotypes observed [91]. Moreover, Zhang *et al.* show that off-target effects are also cell-type specific and depend on the integrity of the DNA repair pathways in this cell type [92].

gRNA	Genic offtarget site	Corresponding gene	Gene function
4	chr. 12	Serine/Threonine kinase 1 (STYK1)	Cell proliferation, differentiation, and survival.
	chr. 6	Origin recognition complex subunit 3 (ORC3)	Initiation of DNA replication
15	chr. 13	Glycerol-3-phosphate deshydrogenase 1 like (GPDL1)	Cardiac sodium current regulation.
	chr. 15	Kinetochore scaffold 1 (KNL1)	Creation of kinetochore microtubule attachments and chromosome segregation.
27	chr. 16	Vesicle amine transport 1 like (VAT1L)	Unknown.
	chr. 15	Ras homology family member V (RHOV)	Control of the actin cytoskeleton.
	chr. 4	Epidermal growth factor transcript variant 3 (EGF)	Cell growth, proliferation, and differentiation

Table 8: Identification and function of genes linked to the potential genic off-targets sites.

Finally, we must be aware that algorithm-based off-targets prediction presents some limitations. The CRISPR MIT software that we used only provides off-target sequences which are closely related to the on-target site, *e.g.*, it fails to predict some off-targets with less similarity. Other methods exist to provide a genome-wide detection of off-target effects (*e.g.*, GUIDE-seq, BLESS, Digenome-seq, etc). However, all these techniques are most of the time performed when the CRISPR/Cas9 system is used for clinical application. In this specific case, safety is a major concern and a genome-wide coverage of all potential off-target effects is crucial to ensure that no mutation occurred. For the use of the CRISPR/Cas9 in basic research, Tsai *et al.* recommend to perform different types of control experiments that allow to rule out potential off-target effects [91]. One possibility is to assess if the initial phenotype (*e.g.*, with a constitutive expression of *ABCB5* in our specific case) is rescued in the ABCB5-knockout cell line after genetic complementation.

2.3 eSpCas9 plasmids construction

We used the eSpCas9 plasmid as expression vector to clone each gRNA. The plasmids were digested with the BbsI restriction enzyme before the ligation with a specific gRNA. The verification of the proper insertion of the gRNA was performed by PCR, followed by sequencing. For each PCR, the reverse PCR primer recognized a common sequence within the eSpCas9 plasmid. However, we chose the antisense oligonucleotide of the inserted gRNA as forward PCR primer in such a way that the PCR is positive only if the gRNA was properly cloned within the eSpCas9 plasmid. The results show a band at the expected size of 200 bp for all the three PCRs (**Figure 13**). Moreover, the sequencing of each PCR product (**Figure 14**) confirms that the amplified sequence perfectly matches with the corresponding gRNA antisense

oligonucleotide, *i.e.*, none mutation occurred during the cloning process. This verification by sequencing was particularly important as the sequence of the gRNA is short, *i.e.* 20 nucleotides. A mutation in one nucleotide would be sufficient to prevent the hybridization of the gRNA to the site of interest but also to increase the number of potential off-target sites.

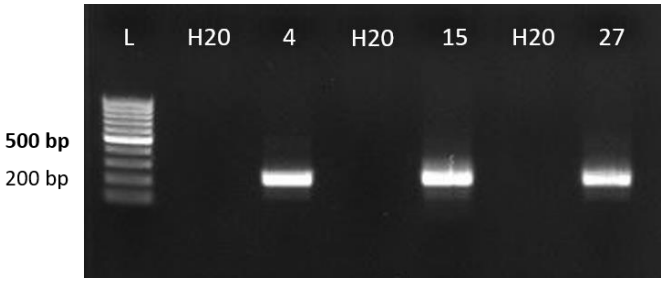

Figure 13: Gel electrophoresis of PCR products using primers for the verification of the proper insertion of the gRNAs into the eSpCas9 plasmid. Ladder (L) 100 bp. Negative control (H2O). gRNA targeting exon 4 (4), 15 (15), or 27 (27) of *ABCB5*. The three PCRs are positive, indicating a proper insertion of the gRNA within the eSpCas9 plasmid (200 bp).

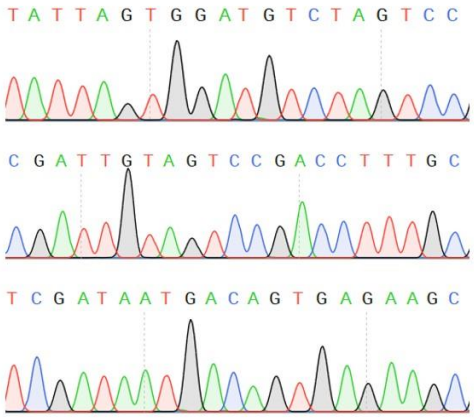

Figure 14: Sequencing of the PCR products to verify the sequence of each gRNA. None mutation was inserted in the gRNA sequence during the step of cloning, as shown by the results of the sequencing: each sequence corresponds to the antisense oligonucleotide (5' - 3') of the gRNA of interest. From the top to the bottom: antisense oligonucleotide from the gRNA targeting exon 4, 15, and 27. The BbsI restriction enzyme sites (AAAC) have not been included in the sequences presented here.

3. ABCB5-knockout: genomic validation

After transfecting cells with the CRISPR/Cas9 system and after selecting these cells with puromycin, we have performed the ABCB5-knockout validation. The validation of a gene-knockout cell line may be performed at three levels: genomic (by screening PCR and sequencing), proteic (by Western Blot), and transcriptomic (by real-time PCR to analyze a potential residual mRNA expression level). We are presenting here the results of the validation of the ABCB5-knockout Mel-Juso cell line at the genomic level. The validation at the proteic level is being performed, but the results are not available yet.

3.1 Polyclonal cell populations

We performed a first screening PCR after cells transfection with the CRISPR/Cas9 system to analyze if the 53 kb or 125 kb fragment was successfully removed in several cells of the polyclonal population. For that purpose, the PCR primers have been chosen in such a way that the result of the PCR is positive only if the deletion occurred: F4 and R15 to detect the 53 kb deletion and F4 and R27 to detect the 125 kb one. Under normal condition, both the reverse and the forward primers are too far from each other to make the amplification possible. In case of deletion, we expect that the mechanism of NHEJ DNA repair links together either the exons 4 and 15 or the exons 4 and 27, making the PCR primers close enough (*i.e.,* separated from ~ 300 bp) to allow the amplification. The results show, for both conditions, a band at the expected size of 300 bp in the pool of transfected cells (TC) (**Figure 15**).

However, we also observed several bands in the wild-type (WT) condition with sizes higher than the one corresponding to the detection of the 125 kb deletion (300 bp). We have assessed the specificity of the F4/R27 pair of primers with the NCBI BLAST tool (available at: https://blast.ncbi.nlm.nih.gov/Blast.cgi). In the genomic database, the webtool identified nine target templates for this pair of primers that may induce non specific amplifications. In addition, the database indicates that all these unintended PCR products have expected lengths higher than 600 bp.

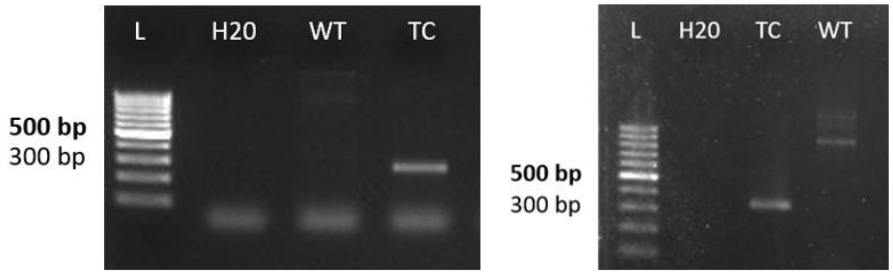

Figure 15: Gel electrophoresis of PCR products using primers for the detection of the 53- or 125 kb deletion. Ladder (L) 100 bp. Negative control (H_20). Wild-type condition (WT). Detection of the 53 kb deletion (left). Pool of transfected cells (TC): positive for the 53 kb deletion (~ 300 bp). Detection of the 125 kb deletion (right). Pool of transfected cells (TC): positive for 125 kb deletion (~ 300 bp).

3.2 Monoclonal cell populations

After detecting the 53 kb and 125 kb deletions in the polyclonal cell populations, the next step was to generate monoclonal cell populations to afterwards select those positive for one of these two deletions. We seeded transfected cells in 96-well plates at a density of one cell per well. After cell growing, we performed again a screening PCR on the collected monoclonal cell populations to identify those positives for the deletion of interest. We carried out a series of three PCRs on each tested clone: one PCR to identify if the 53 kb or 125 kb fragment was removed (following the same protocol than described in **Section 3.1**) and two PCRs to amplify each exon targeted by a gRNA (exons 4 and 15 or exons 4 and 27). Wild-type Mel-Juso cells serve as

negative control for the detection of the 53 kb or 125 kb deletion and as positive control for the amplification of each targeted exon.

53 kb deletion. We screened nine monoclonal cell populations potentially positive for the deletion of 53 kb. The screening identified one positive clone, that we called HE (**Figure 16**). The results show a positive signal at the expected size of ~350 bp in the HE condition, after the PCR performed to detect the 53 kb deletion, indicating that the fragment of 53 kb has probably been removed at least in one of the two alleles of *ABCB5*. The presence of a band at the expected sizes of 270 bp and 275 bp for the exons 4 and 15 confirms a monoallelic deletion of 53 kb in *ABCB5* for the clone HE. In addition, we have sequenced the PCR product of the 53 kb deletion to identify the rattachment between both exons 4 and 15 after the mechanism of NHEJ DNA repair. The sequence was blasted with the NCBI BLAST tool. The database identified in the sequence a part of exon 4 deleted from 28 nucleotides followed by a part of the exon 15 deleted from 23 nucleotides (**Figure S1**).

From these results we conclude that in the clone HE a fragment of 53 kb has been removed from the *ABCB5* gene in one allele. The other allele still contains both exons 4 and 15 indicating that the clone carries a monoallelic deletion of 53 kb in *ABCB5*. A second round of transfection is required to generate biallelic deletion.

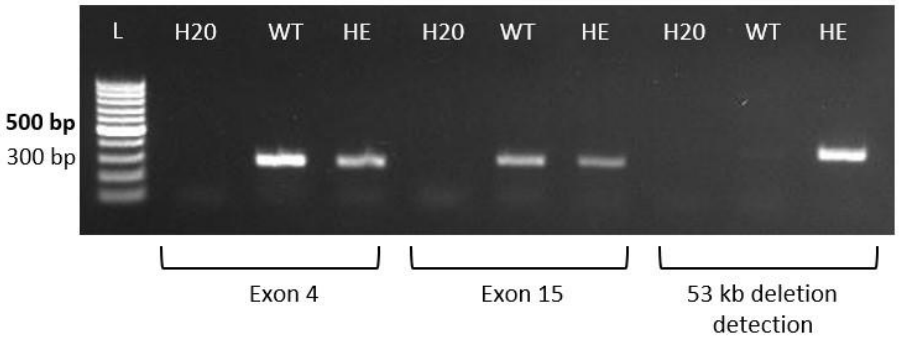

Figure 16: Gel electrophoresis of PCR products using primers for exon 4 and exon 15 amplification, and for the detection of the 53 kb deletion. Ladder (L) 100 bp. Negative control (H_20). Wild-type (WT) condition: positive for exon 4 (270 bp) and exon 15 (275 bp) amplification. Heterozygous (HE) clone: positive for the amplification of exons 4 (270 bp) and 15 (275 bp), and for the detection of the 53 kb deletion (~350 bp).

We performed a second round of transfection on the clone HE in a similar way than for the first transfection. After the generation of monoclonal cell populations, we screened four clones (HO1; HO2; HO3; and HO4) potentially carrying the biallelic deletion of 53 kb in *ABCB5*. The results of the PCR indicate that the four clones tested are homozygous, as shown by: the absence of signal at 270 bp in the four conditions after the amplification of exon 4 (signal present in the wild-type (WT) and heterozygous (HE) conditions); the absence of signal at 275 bp in the four conditions after the amplification of exon 15 (signal present in the WT and HE conditions); and a positive signal at 350 bp in the four conditions after the amplification performed to detect the 53 kb deletion (signal present in the HE but absent in the WT condition) (**Figure 17**). We observe in the HE, HO1, HO2, and HO3 conditions a band at a length that does not correspond to the expected one for the exon 15. As the NCBI BLAST

tool does not identify any unintended target template within the genome for this pair of primers, it is likely that these aspecific bands are related to optimization of the PCR programme.

We conclude that HO1, HO2, HO3, and HO4 have a biallelic deletion of 53 kb in *ABCB5*. A Western Blot is being performed on both Mel-Juso wild-type and ABCB5-knockout Mel-Juso cells to validate these four ABCB5-knockout cell lines at the proteic level.

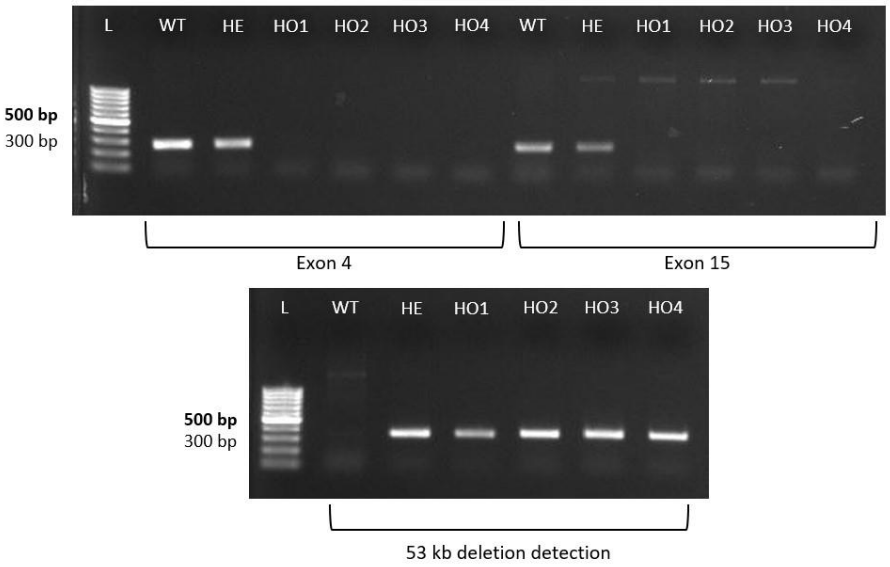

Figure 17: Gel electrophoresis of screening PCR products using primers for exon 4 and exon 15 amplification, and for the detection of the 53 kb deletion. Ladder (L) 100 bp. Wild-type condition (WT): positive for the amplification of exons 4 (270 bp) and 15 (275 bp). Heterozygous clone (HE): positive for the amplification of exons 4 (270 bp and 15 (275 bp), and for the detection of the 53 kb deletion (~350 bp). Homozygous clones (H01, H02, H03, and HO4): positive for the detection of the 53 kb deletion (~350 bp).

125 kb deletion. We screened 30 clones potentially positive for the 125 kb deletion. Two clones were identified as positives, that we called HE1 and HE2 (**Figure 18**). The results show a positive signal at ~300 bp in both the HE1 and HE2 conditions, indicating that the fragment of 125 kb has been removed at least in one of the two alleles of *ABCB5*. The presence of a band at the expected sizes of 270 bp and 280 bp for the exons 4 and 27 confirms the monoallelic deletion of 125 kb on HE1 and HE2. Following the results of the screening PCR, we chose the clone HE1 to perform the future analyses and we kept HE2 in backup. We sequenced the PCR product of the 125 kb deletion to assess the rattachment between both exons 4 and 27 after the cleavage by Cas9 and the mechanism of NHEJ DNA repair. The sequence was blasted with the NCBI BLAST tool and the database identified in the sequence a part of the exon 4 deleted from 38 nucleotides, directly followed by the last 17 nucleotides of the sequence of the exon 27 and the sequence of the intron located after the exon 27 (**Figure S2**).

We conclude that in the HE1 and HE2 clones, a fragment of 125 kb has been removed from the *ABCB5* gene in one allele. The other allele still contains complete exons 4 and 27, indicating that the clones are heterozygous for the 125 kb deletion and

that a second round of transfection is required to obtain biallelic deletion. The latter is being undertaken, but the results are not available yet.

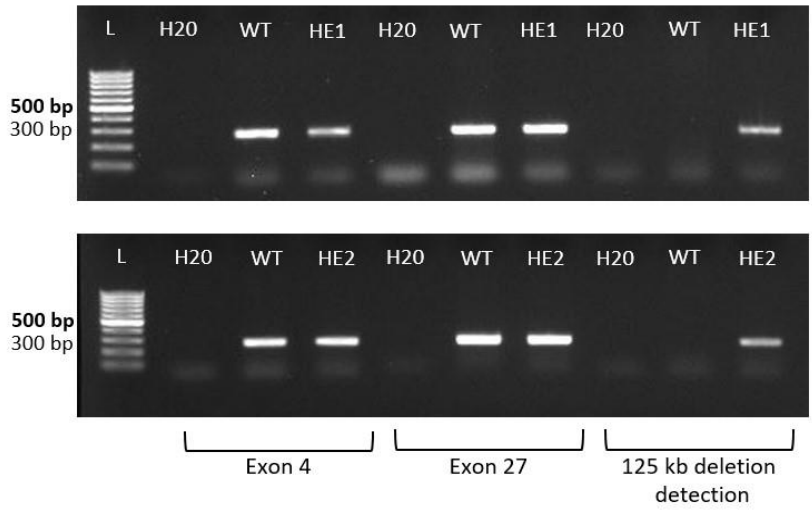

Figure 18: Gel electrophoresis of PCR products using primers for exon 4 and exon 27 amplification, and for the detection of the 125 kb deletion. Ladder (L) 100 bp. Wild-type (WT) condition: positive for the amplification of exons 4 and 27. Heterozygous clones (HE1 and HE2): positive for the amplification of exons 4 and 27, and for the detection of the 125 kb deletion.

4. CRISPR/Cas9: efficiency for large genomic deletion

The main problem of large-scale genomic deletions is that the larger is the size of the fragment to remove, the lower is the efficiency of the CRISPR/Cas9 system. The CRISPR/Cas9 tool is usually used in mammalian cells to produce single-site small indel mutations. Song *et al.* estimate that the efficiency of the method achieves 80% when only one gRNA is employed, but that the efficiency falls to less than 10% when the size of the deletion increases and when several gRNAs are used [89]. The results we obtained after the screening of the monoclonal populations confirm this low efficiency: on the nine clones tested for the 53 kb deletion, only one was identified as positive, giving an efficiency of 11%; on the 30 clones tested for the 125 kb deletion, two were positives, giving an efficiency of 6.7%. Moreover, all these positive clones only carried the large deletion in one of the two alleles of *ABCB5*. The four clones (HO1, HO2, HO3, and HO4) tested after the second transfection with the CRISPR/Cas9 system were all homozygous for the 53 kb deletion, giving an efficiency of 100%. However, this result is not really relevant due to the small sample size. It would be interesting to screen a larger number of clones to get more statistically relevant data about the method efficiency.

Few papers provide methods to increase the efficiency of large genomic deletions using the CRISPR/Cas9 system. Han *et al.* show that the deletion efficiency may be doubled by using two different pairs of gRNAs. However, the major disadvantage of this technique is the increased number of potential off-targets and mutagenesis, which is due to the use of multiple gRNAs. Song *et al.* describe another technique that

currently remains hypothetical. It consists in directly targeting the mechanism of non-homologous end joining DNA repair (NHEJ). They speculate that one of the reasons of the low efficiency of the CRISPR/Cas9-mediated large deletion is the tendency of the fragment deleted to be repaired by the mechanism of NHEJ. They suggest that the use of specific inhibitors targeting key molecules of the DNA repair pathway may decrease the rate of NHEJ repair events and may increase the efficiency of large genomic deletions by the CRISPR/Cas9 system [89].

5. Subcellular fractionation

The second part of this master thesis pursues the study of ABCB5 subcellular localization by the method of cell fractionation. The technique highly depends on the studied cell type and therefore the method may require several attempts to be optimized. As no data are available about previous complete cell fractionation on Mel-Juso cells, we performed a first fractionation on the parental cell line to set up all the parameters of the technique. We are presenting here the results of this first fractionation through the establishment of the distribution profile of a series of enzymes and protein markers. In addition, we carried out a first detection of ABCB5 among the different fractions by Western Blot.

5.1 Distribution profiles of enzymes and protein markers

We followed the protocol described by de Duve *et al.* [85] to perform the fractionation on the Mel-Juso cell line. The method firstly consists in lysing cells in a sucrose solution. Then, centrifugations with increasing speeds is performed to finally recover several fractions enriched in different organelles: nuclear (N), heavy mitochondrial (M), light mitochondrial (L), microsomal (P), and soluble (S) fractions. After collecting the fractions, we established the distribution profile of five enzymes and one protein markers of specific organelles: β-galactosidase (lysosome), alkaline α-glucosidase (endoplasmic reticulum), cytochrome C oxidase (mitochondria), alkaline phosphodiesterase (plasma membrane), dipeptidyl-peptidase III (cytosol), and histone H1 (nucleus).

The results are graphically presented in **Figure 19**. The surface of each block represents the percentage of activity of the enzyme within a fraction, whose the value is listed in the associated table to each graph. The x-axis corresponds to the percentage of proteins (% proteins) within a specific fraction. The y-axis represents the specific relative activity (SRA) of the enzyme within a fraction, also called the enrichment of the enzyme within this fraction. It is calculated by dividing the percentage of activity of the enzyme by the percentage of proteins found in the fraction.

β-galactosidase. The β-galactosidase is a lysosomal enzyme. The lysosomes mainly sediment in the L fraction. The enzymatic dosage detects activity of the β-galactosidase among all the different fractions, with the majority of activity in the L fraction (43.63%). There is an enrichment of the enzyme in the L fraction, as shown by the SRA of 20.64. The enrichment is particularly important: the purity of the fraction is high. Data from previous fractionations in other cell types show that usually the SRA of the β-galactosidase in the L fraction turns around 10. The detection of lysosomal activity in the N fraction (where we expect only to retrieve nuclei) is not coherent and one hypothesis of this result is explained below.

Alkaline α-glucosidase. This enzyme is a marker of the endoplasmic reticulum. The first step of fractionation consists in lysing cells. It induces the break of the endoplasmic reticulum that subsequently forms small vesicles called microsomes. As these vesicles mainly sediment in the P fraction which contains the majority of the

microsomes, we expect to retrieve most of the alkaline α-glucosidase activity in this specific fraction. However, the results show a distribution of the enzymatic activity among all the fractions with the greatest activity in the N fraction (37.88%) followed by the P fraction (22.10%). We speculate that the high percentage in N may be due to large amounts of rough reticulum endoplasmic (RER) that continuous the outer nuclear membrane or to insufficient cell lysis (described below). Finally, we do not observe any significant enrichment of the enzyme within one of the five fractions, as shown by the quite similar SRA among the N, M, L, and P fractions (1.41; 2.43; 2.15; and 1.53 respectively). Unlike the β-galactosidase, the alkaline α-glucosidase does not present a very specific distribution profile.

Cytochrome C oxidase. The cytochrome C oxidase is a marker of mitochondria. This organelle may be subdivided between heavy- and light mitochondria. The heavy mitochondria are larger in size and volume. They have a higher sedimentation coefficient and are consequently mainly retrieved within the M fraction [93]. The light mitochondria are smaller in size and volume, and are usually collected in the L fraction. The results show a majority of cytochrome C oxidase activity within the M fraction (59.67%) and an enrichment of the enzyme within this specific fraction (SRA of 7.29). Although the enzymatic activity is low in the L fraction (6.92%), the enrichment of the enzyme within the fraction is 3.27. Finally, the detection of cytochrome C oxidase in the N fraction is less coherent, but one hypothesis about this result is described below.

Alkaline phosphodiesterase. This enzyme is a marker of the plasma membrane. Similarly to the endoplasmic reticulum, the step of cell lysis promotes the break of plasma membranes that subsequently form small vesicles. These vesicles may vary in size, *i.e.* the distribution profile of the alkaline phosphodiesterase is variable and depends on the intensity of cell lysis. However, in most cases, these plasma membrane vesicles sediment in the P fraction in which we find the microsomes. Our results are consistent with these data, as shown by the majority of alkaline phosphodiesterase activity detected in the P fraction (32.02%). However, we also detect activity in the heavier fractions (L, M, and N), with an enrichment of the enzyme in the L fraction (SRA of 8.43). The presence of plasma membrane in both M and L fractions may be due to larger plasma membrane vesicles that have sedimented in these specific fractions. The detection of alkaline-phosphodiesterase activity in the N fraction is less coherent and one hypothesis for this result is described below.

Dipeptidyl-peptidase III. This enzyme is a soluble enzyme found in the cytosol: we expect to detect the majority of enzymatic activity in the S fraction that contains all the non-sedimentable particles. The results show a high percentage of activity in this S fraction (65.71%). However, we also detect some activity in all the other fractions. One hypothesis for the presence of dipeptidyl-peptidase III in both the M and L fractions is the presence of autophagic vesicles. During the process of autophagy, a part of the cytosol is bundled within autophagic vesicles that belongs to the lysosomal system, *i.e.*, they mainly sediment in the M and L fractions. It is possible that the vesicle cargo contains a certain amount of dipeptidyl-peptidase III, explaining the presence within these fractions. However, the presence of enzymatic activity in the N fraction is less coherent and is explained below.

Histone H1. The histone H1 is a protein marker of the nucleus which can be detected by Western Blotting. We have detected the histone H1 protein at the expected size of 37 kDa with an anti-histone H1 monoclonal antibody. The results show an intense signal size in the N fraction and a very low signal in the M and P fractions. The E fraction corresponds to the supernatant recovered after the first step of centrifugation, *i.e.,* all the cell lysate without the nuclei. The absence of detection of histone H1 in the E fraction is consistent and indicates that the nuclei have been entirely separated from the cell lysate. Following the Western Blot, we have quantified the histone H1 signals using the ImageJ software to graphically obtain the distribution profile of the protein marker. The amount of protein is almost entirely found in the N fraction, with a percentage of 98.71%.

Regarding these results, we have identified one parameter to optimize for the future fractionations of the Mel-Juso cell line. We have detected for all enzyme markers a percentage of activity in the N fraction. We hypothetize that it is due to the presence of unbroken cells in this specific fraction. We performed two series of six passages in the Dounce homogeneizer to lyse the cells but this number is probably insufficient to lyse all the cells. For the next fractionation, we will slightly increase this number to ten passages. However, it is important to be aware that each cell type presents different degree of sensitivity to the mechanism of lysis. The process must be carefully balanced: if the lysis is too strong, the risk is to also break the nucleus and to release fragments of DNA within all the different fractions. Finally, we could also establish the distribution profile of the Golgi apparatus and the peroxisome. Specific enzyme markers exist for these two organelles, *i.e.* the galactosyl transferase and the catalase.

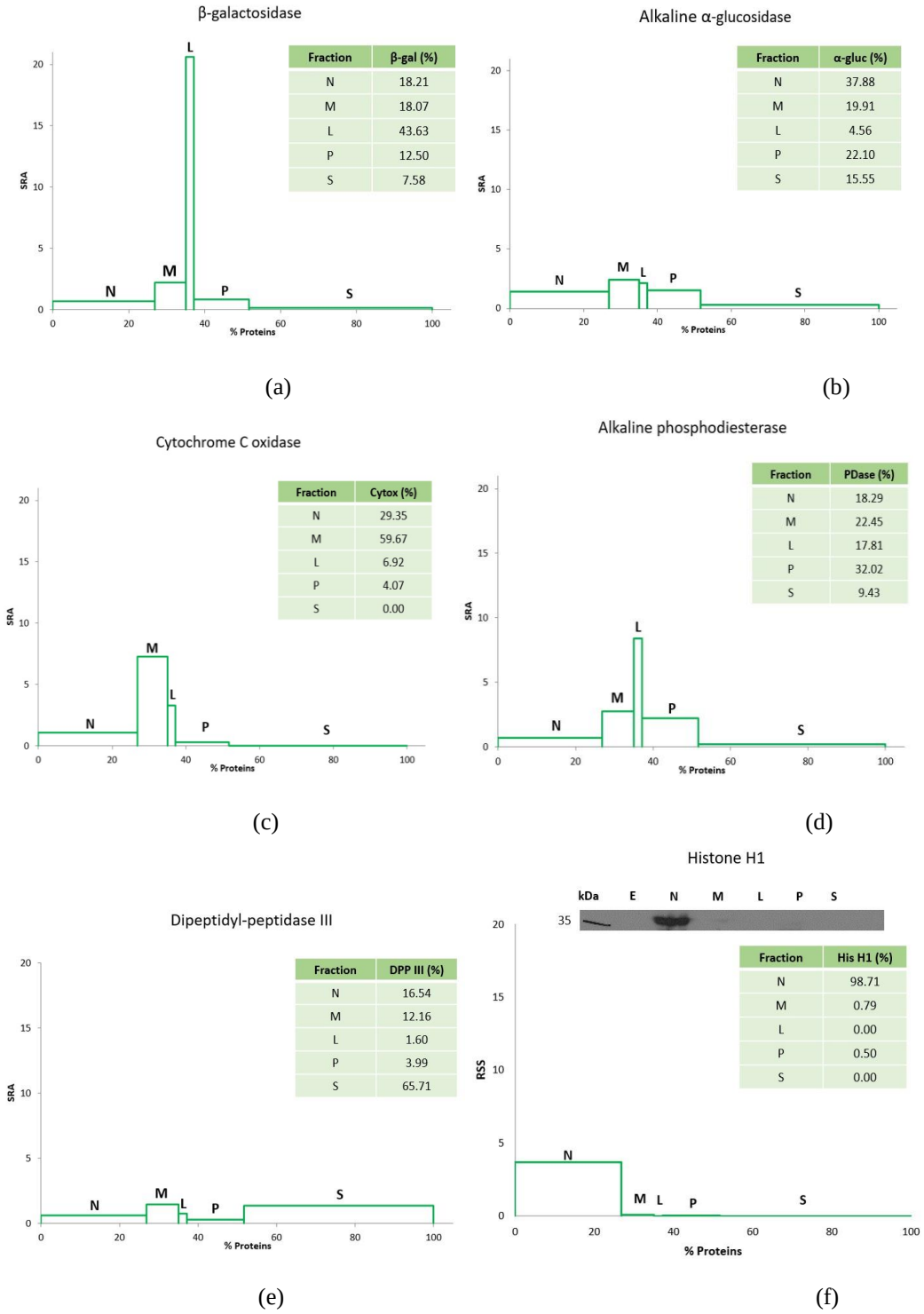

Figure 19: Subcellular fractionation on Mel-Juso parenteral cells by differential centrifugation. Series of enzymatic assays to establish the distribution profile of the *β*-galactosidase (lysosome) (a), the alkaline *α*-glucosidase (endoplasmic reticulum) (b), the cytochrome C oxidase (mitochondria) (Cytox), the alkaline phosphodiesterase (plasma membrane) (d), and the dipeptidyl-peptidase III (cytosol) (e) among the different fractions. Western Blotting and quantification by ImageJ to establish the distribution profile of histone H1 (nucleus) (f). x-axis: percentage of proteins (% proteins) within a specific fraction; y-axis: specific relative activity (SRA) of the enzyme within the fraction, *i.e.* the enrichment of the enzyme in this specific fraction. Calculated by dividing the percentage of activity of the enzyme by the percentage of proteins within the fraction. y-axis for histone H1: relative specific signal (RSS) as the protein does not have enzymatic activity. Surface of each block: percentage of

activity of the enzyme within a specific fraction. The percentage are listed in the associated table for each enzymatic dosage.

5.2 Distribution profile of ABCB5

The results of the real-time PCR have shown that Mel-Juso cells at least express *ABCB5* under the *β* isoform (**Section 1.1**). The size of the protein is estimated at 90 kDa and we have performed a Western Blot to detect the ABCB5 protein among the different fractions. The anti-ABCB5 polcylonal antibody (Rockland, 600-401-A77S) was used to identify the protein.

The results show a band at 90 kDa in the cell lysate (E) and in the nuclear (N) and microsomal (P) fractions (**Figure 20**). The complete absence of signal in the L fraction indicates that ABCB5*β* is probably not a lysosomal transmembrane protein. We hypothetize that the transporter is at least located in the nuclear membrane, as shown by the intense signal observed in the N fraction that contains the majority of the nuclei. These data are supported by previous studies that identified another ABC transporter (ABCB1) in the nuclear membrane of human breast cancer cells (MCF-7) and human colon cells (LoVo cell line) [94, 95]. As both ABCB1 and ABCB5 have 73% of structure homology, it is plausible that ABCB5 is found within the nuclear membrane. The detection of ABCB5 in the P fraction only provides insights about potential other subcellular localizations of the transporter. This fraction contains the majority of microsomes that originate from fragments of the plasma membrane, the endoplasmic reticulum, but also the Golgi apparatus. It would be relevant to perform a sub-fractionation on this specific fraction (*e.g.,* by using a sucrose density gradient separation) to isolate each organelle and more precisely define the localization of ABCB5. Moreover, early melanosomes could also be present in the P fraction. It would be interesting to establish the distribution profile of the organelle among all the fractions by using the gp100 glycoprotein as protein marker. As Chen *et al.* have already hypothetized that ABCB5 could be involved in melanogenesis, we cannot exclude that the transporter is located within this specific organelle [65].

However, we must carrefully interpret these data and must be aware that it remains hypothetical. The anti-ABCB5 antibody used shows a lack of specificity and recognizes many other proteins. Even if these results are consistent with those previously described by Sana *et al.* (*i.e.,* a mixed localization of ABCB5 both in N and P fractions), we cannot conclude that the observed bands correspond to ABCB5. Until now, there is no trustworthy ABCB5 negative control in mammalian cells to prove the specificity of this antibody.

These results show the interest to use, in this specific case, the ABCB5-knockout cell line as a robust negative control. As already mentioned, the validation at the proteic level of the ABCB5-knockout cell line by Western Blot is being performed. This Western Blot is simultenaeously performed on ABCB5-expressing and ABCB5-knockout Mel-Juso cells. We expect that the synthesis of ABCB5 is completely inhibited in the knockout cell line. Thereby, the specificity of the anti-ABCB5 antibody will be validated if we detect a signal at 90 kDa in the ABCB5-expressing cells that is absent from the ABCB5-knockout cell line. Afterwards, the purpose is to

perform a second fractionation simultaneously on both ABCB5-expressing and ABCB5-knockout cells to strenghten and validate the data about the localization of the transporter among the different fractions.

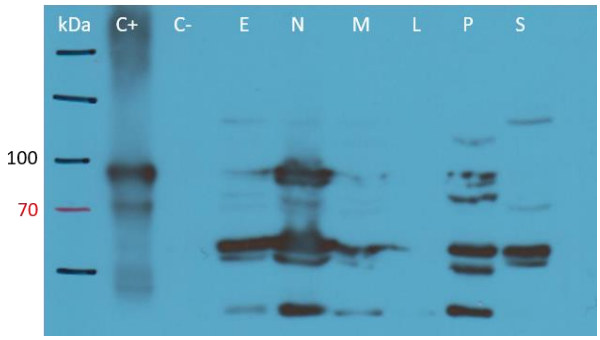

Figure 20: Detection of ABCB5 by Western Blotting following Mel-Juso subcellular fractionation. Detection of ABCB5β (90 kDa) using the anti-ABCB5 polyclonal antibody from Rockland (600-401A77S). Ladder (kDa); ABCB5β transfected-High-5 insect cells as positive control (C+); non-transfected High-5 insect cells as negative control (C-). Mel-Juso cell lysate (E), nuclear (N), heavy mitochondrial (M), light mitochondrial (L), microsomal (P), and soluble (S) fractions.

Other techniques have already been tested to detect the ABCB5 transporter without the need to use anti-ABCB5 antibodies. Specific tags such as the eGFP can be used to generate a fusion protein with the ABCB5 transporter. However, such a large tag can render the protein non-functional and bias its localization. Therefore, we decided to work from the native protein.

The firm Promega has developed a method called Nano-Glo HiBiT blotting system. The method allows to easily visualize HiBiT-tagged proteins on a membrane, after gel separation. For that, a blotting reagent containing both the LgBiT protein and the furimazine substrate is added to the membrane. The HiBiT tag is able to bind with high affinity to the LgBiT protein that together form a complex having a luciferase activity. In presence of the furimazine substrate, the complex releases a luminescence signal that can be detected on the membrane. This alternative technique might be powerful to detect the ABCB5 transporter without the use of anti-ABCB5 antibodies. Compared to other existing tags, the HiBiT tag has several advantages: the small size of the tag (1.3 kDa) allows to directly insert it within the endogenous protein thanks to the CRISPR/Cas9 tool, meaning that the technique does not require cloning procedures; the size of the tag decreases the risk of changes in the protein conformation that may lead to protein mislocalization. Moreover, the technique is highly sensitive and quantitative as the luminescence signal is directly proportional to the luciferase activity. Finally, in contrary to anti-ABCB5 antibodies that recognize many other proteins, the background noise with this alternative technique would be probably very low.

Conclusions and perspectives

1. ABCB5-knockout cell line

The first part of this master thesis aimed to generate an ABCB5-knockout cell line to use it as a tool to pursue the characterization of the ABCB5 transporter. We chose as model the Mel-Juso unpigmented primary melanoma cells that at least expresses the ABCB5 transporter under the β isoform. We employed the CRISPR/Cas9 genome-editing tool to remove either a fragment of 53 kb or 125 kb in the *ABCB5* gene. For that purpose, three guide RNAs have been designed with high on-target specificity and low risk of off-target effects. After a first round of transfection, clonal expansion, and screening PCR we achieved to generate clones with a monoallelic deletion of 53 kb or 125 kb in *ABCB5*. A second round of transfection allowed us to successfully recover four clones with a biallelic deletion of 53 kb. To date, these clones have been validated at the genomic level (by screening PCR and sequencing). The validation at the proteic level (by Western Blot) is currently being undertaken to confirm that the protein synthesis of both the ABCB5 full-length and β isoforms is inhibited. The second transfection that will provide a Mel-Juso cell line with a biallelic deletion of 125 kb is in progress. This cell line will be entirely depleted from the *ABCB5* gene, preventing both the mRNA transcription and the protein synthesis. These two parameters will be validated by Western Blot and real-time PCR.

Our results demonstrate that the CRISPR/Cas9 is a powerful tool to precisely edit and modify genes of interest, thanks to the design of specific gRNAs. Although most of the studies in mammalian cells used the CRISPR/Cas9 tool to induce small indel mutations at single-site, we have shown that it is also suitable to remove large-scale genomic regions from over 100 kb. This purpose may be achieved by co-transfecting cells with several gRNAs.

The ABCB5-knockout Mel-Juso cell line constitutes a powerful model that open the field to new research to characterize the ABCB5 transporter, mainly by loss-of-function gene studies. As previously mentioned, the role of ABCB5 in melanoma chemoresistance has been well described: the transporter mediates the efflux of a wide range of anti-cancer drugs out of the cell. However, there is now emerging evidence of an additional role of ABCB5 in melanomagenesis. This role in tumorigenesis would be drug-efflux independent and directly related to the efflux of endogenous substrates such as metabolites, signaling molecules, etc. To date, data remain controversial: some papers describe ABCB5 as an oncogene, promoting tumor progression and metastases; other studies suggest that ABCB5 acts as a tumor suppressor, preventing tumor initiation through the inhibition of cell proliferation. However, we cannot exclude that the role of ABCB5 in melanomagenesis is cell type specific: the oncogenic role of ABCB5 has been described in a population of malignant-melanoma initiating cells (MMICs) although the role as tumor suppressor in non-MMICs.

It will be interesting to perform a series of functional assays on both the ABCB5-expressing and ABCB5-knockout Mel-Juso cell lines to identify a role of ABCB5 as tumor suppressor in this specific cell type. Proliferation assays, anchorage independent growth assays, migration and invasion assays, etc. are all tests that can be performed

in vitro to study some hallmarks of cancer and elucidate the role of ABCB5 in melanomagenesis. Before starting all these functional assays, one important step is to sequence all the off-targets sites to detect potential mutations that could interfere with the results of the analyses.

Another interesting field would be to study the role of ABCB5 in the adaptation of cancer cells metabolism. This adaptation is directly related to the tumor environment (*e.g.,* hypoxia) and is essential for tumor growth, survival, proliferation, and maintenance. Among those, increasing the rate of glycolysis and limiting oxidative phosphorylation is one of the most frequent mechanism of adaptation and is known as the Warburg effect [96]. In 2016, Lutz *et al.* established the metabolic profiles for two groups of human G3361 malignant-melanoma initiating cell lines: the first condition expressing ABCB5 and the second one knockdown for the transporter expression by the use of shRNA. The results showed significantly higher levels of several compounds involved in the glycolytic pathway in the ABCB5-expressing G3361 melanoma cells compared to the ABCB5-knockdown condition, suggesting a potential role of ABCB5 in increasing the rate of the glycolytic pathway in this specific subpopulation of cancer stem cells. The molecular mechanism remains unclear but researchers suggest that this upregulation may result from an ABCB5/IL-1β/HIF-1α/PFKP signaling cascade. The metabolomic analysis has been carried out on the G3361 malignant-melanoma initiating cells (*i.e.,* cancer stem cells) and researchers pointed out the interest to perform a similar study on additional melanoma cell lines expressing ABCB5. As the Mel-Juso cells are not cancer stem cells, this kind of study will allow to assess if the effects of ABCB5 on the cellular metabolism are similar or different from those observed in the G3361 cell line.

Here we have shown that studying the role of ABCB5 in melanomagenesis is one example of all the potential applications that provides the generation of the ABCB5-knockout MelJuso cell line. Other fields of research may be explored such as: drug-sensitivity assays, substrates transport assay, proteomic analysis, etc.

2. ABCB5 subcellular localization

The second part of this Master Thesis aimed to study the ABCB5 subcellular localization by the method of cell fractionation described by de Duve *et al.*. As the technique highly depends on the studied cell type, we performed a first fractionation on the parental Mel-Juso cell line to set up and optimize all the parameters of the technique. After lysing the cells in sucrose solution, we used sequentially increasing speeds of centrifugation to recover a total of five fractions enriched in specific organelles: nuclear (N), heavy mitochondrial (M), light mitochondrial (L), microsomal (P), and soluble (S) fractions. A series of enzymatic assays and one immunoblotting allowed us to establish the distribution profiles of enzyme and protein markers of specific organelles through the different fractions.

Overall, the results have shown a coherent distribution profile of these enzymes and protein markers, but the detection in the nuclear fraction of activity for all the tested enzymes seems to indicate the presence of intact cells in this specific fraction. For the future fractionations, a slight increase from six to ten in the number of Dounce

passages will probably be sufficient to lyse all the cells without the risk to also break nuclei.

In addition, we have established a first distribution profile of ABCB5 after identifying the protein by Western Blot. We have detected an enrichment of ABCB5 both in the nuclear and microsomal fractions suggesting that ABCB5 has a mixed localization. Further steps of purification would be necessary in the P fraction to better define the transporter localization in the endoplasmic reticulum, the plasma membrane, the Golgi apparatus, or the early melanosomes. Even if these results are consistent with data from previous cell fractionation, they remain hypothetical. The anti-ABCB5 antibody used presents a lack of specificity for the transporter, as shown by the recognition of many other proteins. A trustworthy negative control in mammalian cells is needed to prove and validate the specificity of this antibody. Our engineered ABCB5-knockout Mel-Juso cell line constitutes a robust tool to assess this specificity. The proteic validation (*i.e.* by Western Blot) of the ABCB5-knockout cell line is being undertaken and will allow us to prove the specificity of the antibody. Afterwards, a second set of fractionations will be carried out simultaneously on both the ABCB5-expressing and ABCB5-knockout Mel-Juso cell line to strenghten the data about the transporter localization. However, we also have considered other methods to detect the ABCB5 transporter, without the need to use anti-ABCB5 antibodies. Among those, the HiBiT technique developed by Promega could be suitable and could constitute a relevant alternative because the method is highly sensitive and quantitative.

The cell fractionation by differential centrifugation (*i.e.* de Duve's method) gets a first insight about the transporter localization, by determining which fractions are enriched for ABCB5. However, this technique does not provide pure organelles fractions and we will perform further steps of purification using equilibrium density-gradient centrifugation. The method separates the organelles according to their density. It consists in establishing a sucrose density gradient and to subject the fraction to a very high centrifugal force (usually 15,000 g). The organelles sediment until they reach the layer of the sucrose gradient corresponding to their own density. The technique is useful to separate the rough endoplasmic reticulum from the Golgi apparatus and the plasma membrane. This property is particulary interesting as these organelles are mainly found in the microsomal fraction (P), in which we hypothetize that ABCB5 is also localized.

Finally, we must bear in mind that the subcellular localization of ABCB5 could be cell specific. Identifying the localization of ABCB5 in Mel-Juso cells will help to better understand the role of the transporter in melanoma cells. However, the transporter is also expressed in other cell types (*e.g.*, human testis), in which we cannot exclude a different subcellular localization of the transporter. The subcellular localization of ABCB5 is crucial to further study the role of the transporter at the intracellular level, to assess potential interactions of ABCB5 with other proteins, etc.

This Master Thesis will have contributed to pave the way toward the characterization of the ABCB5 transporter in engineering an ABCB5-knockout human melanoma cell line, which will be used as a robust negative control.

References

[1] M. Dean, A. Rzhetsky, and R. Allikmets. The Human ATP-Binding Cassette (ABC) Transporter Superfamily. *Genome Research*, 11(7):1156–66, 2001.

[2] S. Wilkens. Structure and mechanism of ABC transporters. *F1000Prime Reports*, 7:14, 2015.

[3] V. Vasiliou, K. Vasiliou, and D.W. Nebert. Human ATP-binding cassette (ABC) transporter family. *Human Genomics*, 3(3):281–90, 2009.

[4] F.L. Theodoulou and I.D. Kerr. ABC transporter research: going strong 40 years on. *Biochemical Society transactions*, 43(5):1033–40, 2015.

[5] J.P. Gillet, T. Efferth, and J. Remacle. Chemotherapy-induced resistance by ATPbinding cassette transporter genes. *Biochemica et Biophysica Acta Reviews on Cancer*, 1775(2):237–342, 2007.

[6] R.W. Robey, K.M. Pluchino, M.D. Hall, A.T. Fojo, S.E. Bates, and M.M. Gottesman. Revisiting the role of ABC transporters in multridug-resistant cancer. *Nature Reviews Cancer*, 18(7):452–64, 2018.

[7] V. Kolovou, A. Marvaki, M. Boutsikou, G. Vasilopoulos, D. Degiannis, C. Marvaki, and G. Kolovou. Effect of ATP-binding Cassette Transporter A1 (ABCA1) Gene Polymorphisms on Plasma Lipid Variables and Common Demographic Parameters in Greek Nurses. *The Open Cardiovascular Medicine Journal*, 10:233–39, 2016.

[8] J.R. Riordan, K. Deuchars, N. Kartner, N. Alon, J. Trent, and V. Ling. Amplification of P-glycoprotein genes in multidrug-resistant mammalian cell lines. *Nature*, 316:817–19, 1985.

[9] L.M. Hodges, S.M. Markova, L.W. Chinn, J.M. Gow, D.L. Kroetz, T.E. Klein, and R.B. Altman. Very important pharmacogenes summary: ABCB1 (MDR1, P-glycoprotein). *Pharmacogenetics and genomics*, 21(3):152–61, 2011.

[10] F. Zhang, W. Zhang, L. Liu, C.L. Fisher, D. Hui, S. Childs, K. Dorovini-Zis, and V. Ling. Characterization of ABCB9, and ATP-binding cassette protein associated with lysosomes. *The Journal of Biological Chemistry*, 275(30):23287–94, 2000.

[11] F.G. Russel, J.B. Koenderink, and R. Masereeuw. Multidrug resistance protein 4

(MRP4/ABCC4: a versatile efflux transporter for drugs and signaling molecules. *Trends in Pharmacological Sciences*, 29(4):200–7, 2008.

[12] J.F. Hunt, C. Wang, and R.C. Ford. Cystic Fibrosis Transmembrane Conductance Regulator (ABCC7) Structure. *Cold Spring Harbor perspectives in medicine*, 3(2), 2013.

[13] D. Sheppard and M. Welsh. Structure and Function of the CFTR Chloride Channel.
Physiological Reviews, 79(1 Suppl.):S23–45, 1999.

[14] J. Bryan, A. Munoz, X. Zhang, M. Düfer, G. Drews, P. Krippeit-Drews, and L. AguilarBryan. ABCC8 and ABCC9: ABC transporters that regulate K+ channels. *European Journal of Physiology*, 453(5):703–18, 2007.

[15] S.M. Wilcox, H. Arora, L. Munro, J. Xin, F. Fenninger, L.A. Johnson, C.G. Pfeifer, K. Bok Choi, J. Hou, P.A. Hoodless, and W.A. Jefferies. The role of the innate immune response regulatory gene ABCF1 in mammalian embryogenesis and development. *PLoS One*, 12(5):e0175918, 2017.

[16] S. Velamakanni, S. Wei, T. Janvilisri, and H. van Veen. ABCG transporters: structure, substrate specificities and physiological roles. *Journal of Bioenergetics and Biomembranes*, 39(5-6):465–71, 2007.

[17] J.I. Fletcher, M. Haber, M.J. Henderson, and M.D. Norris. ABC transporters in cancer: more than just drug efflux pumps. *Nature Reviews Cancer*, 10(2):147–56, 2010.

[18] R-R. Begicevic and M. Falasca. ABC Transporters in Cancer Stem Cells: Beyond Chemoresistance. *International Journal of Molecular Sciences*, 18(11):2362, 2017.

[19] M.M. Gottesman, L.J. Goldstein, A. Fojo, H. Galski, and I. Pastan. Expression of the Multidrug Resistance Gene in Human Cancer. *Journal of the National Cancer Institute*, 81(2):116–24, 1989.

[20] L. Amiri-Kordestani, A. Basseville, K. Kurdziel, A. Tito Fojo, and S.E. Bates. Targeting MDR in Breast and Lung Cancer: Discriminating its Potential Importance from the Failure of Drug Resistance Reversal Studies. *Drug Resistance Updates*, 15(1-2):50–61, 2012.

[21] T. Kawanobe, S. Kogure, S. Nakamura, M. Sato, K. Katayama, J. Mitsuhashi, K. Noguchi, and Y. Sugimoto. Expression of human ABCB5 confers resistance to taxanes and anthracyclines. *Biochemical and Biophysical Research Communications*, 418:736–41, 2012.

[22] M. Hosseni Hasanabady and F. Kalalinia. ABCG2 inhibition as therapeutic approach for overcoming multidrug resistance in cancer. *Journal of Biosciences*, 41(2):313–24, 2016.

[23] J.I. Fletcher, R.T. Williams, M.J. Henderson, M.D. Norris, and M. Haber. ABC transporters as mediators of drug resistance and contributors to cancer cell biology. *Drug Resistance Updates*, pages 1–9, 2016.

[24] S. Copsel, C. Garcia, F. Diez, M. Vermeulen, A. Baldi, L. Blanciotti, F. Russel, C. Shayo, and C. Davio. Multidrug Resistance Protein 4 (MRP4/ABCC4) Regulates cAMP Cellular Levels and Controls Human Leukemia Cell Proliferation and Differentiation. *The Journal of Biological Chemistry*, 286(9):69–79, 2011.

[25] M. Henderson, M. Haber, A. Porro, M. Munoz, N. Iraciand C. Xue, J. Murray, C. Flemming, J. Smith, J. Fletcher, S. Gherardi, C-K. Kwek, A. Russell, E. Valli, W. London,
A. Buxton, L. Ashton, A. Sartorelli, S. Cohn, M. Schwab, G. Marshall, G. Perini, and M. Norris. ABCC Multidrug Transporters in Childhood Neuroblastoma: Clinical and Biological Effects Independent of Cytotoxic Drug Efflux. *Journal of the National Cancer Institute*, 103(16):1236–51, 2011.

[26] Y. Mochida, K. Taguchi, S. Taniguchi, M. Tsuneyoshi, H. Kuwano, T. Tsuzuki, M. Kuwano, and M. Wada. The role of P-glycoprotein in intestinal tumorigenesis: disruption of suppresses polyp formation in a*pc*Min/+ mice. *Carcinogenesis*, 24(7):1219– 24, 2003.

[27] E. Hedditch, B. Gao, A. Russell, C. Emmanuel, and M. Henderson. ABCA transporter gene expression and poor outcome in epithelial ovarian cancer. *Journal of the National Cancer Institute*, 106(7), 2014.

[28] J. Ferlay, M. Colombet, I. Soerjomataram, T. Dyba, G. Randi, M. Bettio, A. Gavin, O. Visser, and F. Bray. Cancer incidence and mortality patterns in Europe: Estimates for 40 countries and 25 major cancers in 2018. *European Journal of Cancer*, 103:356–87, 2018.

[29] A.L. Isola, K. Eddy, and S. Chen. Biology, Therapy and Implications of Tumor Exosomes in the Progression of Melanoma. *Cancers*, 8(12):110, 2016.

[30] A.H. Shain and B.C. Bastian. From melanocytes to melanomas. *Nature Reviews Cancer*, 16(6):347–58, 2016.

[31] G. Palmieri, M. Ombra, M. Colombino, M. Casula, M. Sini, A. Manca, P. Paliogiannis, P. Antonio Ascierto, and A. Cossu. Multiple molecular pathways in melanomagenesis:
characterization of therapeutic targets. *Frontiers in Oncology*, 5(183), 2015.

[32] E. Erdei and S.M. Torres. A new understanding in the epidemiology of melanoma. *Expert Review of Anticancer Therapy*, 10(11):1811–23, 2010.

[33] M. Rastrelli, S. Tropea, C. Riccardo Rossi, and M. Alaibac. Melanoma: Epidemiology, Risk Factors, Pathogenesis, Diagnosis and Classification. *In Vivo*, 28(6):1005–11, 2014.

[34] J. D'Orazio, S. Jarrett, A. Amaro-Ortiz, and T. Scott. UV Radiation and the Skin. *International Journal of Molecular Sciences*, 14:12222–48, 2013.

[35] M. Watson, D. Holman, and M. Maguire-Eisen. Ultraviolet Radiation Exposure and Its Impact on Skin Cancer Risk. *Seminar in Oncology Nursing*, 32(3):241–54, 2016.

[36] R.J. Sullivan and D.E. Fisher. Understanding the biology of melanoma and therapeutic implications. *Hematology/Oncology Clinics of North America*, 28(3):437–53, 2014.

[37] A. Joosse, E. de Vries, R. Eckel, T. Nijsten, A. Eggermont, D. Holzel, J. Willem W. Coeberg, and J. Engel. Gender Differences in Melanoma Survival: Female Patients

Have a Decreased Risk of Metastasis. *Journal of Investigative Dermatology*, 131:719– 26, 2011.

[38] C. Bevona, W. Goggins, T. Quinn, J. Fullerton, and H. Tsao. Cutaneous Melanoma Associated With Nevi. *Archives of dermatology*, 139(12):1620–4, 2003.

[39] S. Gandini, F. Sera, M.S. Cattaruzza, P. Pasquini, D. Abeni, P. Boyle, and C.F. Melchi. Meta-analysis of risk factors for cutaneous melanoma: I. Common and atypical naevi. *European Journal of Cancer*, 41:28–44, 2005.

[40] E. Soura, P. Eliades, K. Shannon, A. Stratigos, and H. Tsao. Hereditary Melanoma: Update on Syndromes and Management - Genetics of familial atypical multiple mole melanoma syndrome. *Journal of the American Academy of Dermatology*, 74(3):395–407, 2016.

[41] T. Kondo and V. Hearing. Update on the regulation of mammalian melanocyte function and skin pigmentation. *Expert Review of Dermatology*, 6(1):97–108, 2011.

[42] M. Takata, H. Murata, and T. Saida. Molecular pathogenesis of malignant melanoma:
a different perspective from the studies of melanocytic nevus and acral melanoma. *Pigment Cell Melanoma Research*, 23:64–71, 2009.

[43] E. Castellano and J. Downward. RAS Interaction with PI3K: More Than Just Another Effector Pathway. *Genes Cancer*, 2(3):261–74, 2011.

[44] E. Muñoz-Couselo, E. Adelantado, C. Ortiz, J. Garcia, and J. Perez-Garcia. NRASmutant melanoma: current challenges and future prospect. *OncoTargets and Therapy*, 10:3941–47, 2017.

[45] M. Davies and Y. Samuels. Analysis of the genome to personalize therapy for melanoma. *Oncogene*, 29(41):5545–55, 2010.

[46] N. Leslie and C. Downes. PTEN function: how normal cells control it and tumour cells lose it. *Biochemical Journal*, 382(Pt 1):1–11, 2004.

[47] K. Cichowski, S. Santiago, M. Jardim, B. Johnson, and T. Jacks. Dynamic regulation of the Ras pathway via proteolysis of the NF1 tumor suppressor. *Genes and Development*, 17(4):449–54, 2002.

[48] M. Kiuru and K. Busam. The NF1 gene in tumor syndromes and melanoma. *Laboratory Investigation*, 97(2):146–57, 2017.

[49] V. Hill, J. Gartner, Y. Samuels, and A. Goldstein. The Genetics of Melanoma: Recent Advances. *Annual Review of Genomics and Human Genetics*, 14:257–79, 2013.

[50] H. Dralle, A. Machens, J. Basa, V. Fatourechi, S. Franceschi, I. Hay, Y. Nikiforov, F. Pacini, J. Pasieka, and S. Sherman. Follicular cell-derived thyroid cancer. *Nature Reviews Disease Primers*, 1(15077), 2015.

[51] S. Wu and R.K. Singh. Resistance to Chemotherapy and Molecularly Targeted Therapies: Rationale for Combination Therapy inMalignant Melanoma. *Current Molecular Medicine*, 11(7):553–63, 2011.

[52] P. Strojan. Role of radiotherapy in melanoma management. *Radiology and Oncology*, 44(1):1–12, 2010.

[53] A.S. Yang and P.B. Chapman. The History and Future of Chemotherapy for Melanoma. *Hematology/Oncology Clinics of North America*, 23(3):583–602, 2009.

[54] J. Haanen. Immunotherapy of melanoma. *European Journal of Cancer Supplements*, 11(2):97–105, 2013.

[55] A.A. Tarhini, H. Gogas, and J.M. Kirkwood. IFN-α in the Treatment of Melanoma. *The Journal of Immunology*, 189(8):3789–93, 2012.

[56] S. Bhatia, S. Tykodi, and J. Thompson. Treatment of Metastatic Melanoma: An Overview. *Oncology*, 23(6):488–96, 2009.

[57] A.K. Karlsson and S.N. Saleh. Checkpoint inhibitors or malignant melanoma: a systematic review and meta-analysis. *Clinical, Cosmetic and Investigational Dermatology*, 10:325–39, 2017.

[58] E. Buchbinder and A. Desai. CTLA-4 and PD-1 Pathways: Similarities, Differencies, and Implications of Their Inhibition. *American Journal of Clinical Oncology*, 39(1):98– 106, 2016.

[59] S.M. Goldinger, C. Murer, P. Stieger, and R. Dummer. Targeted therapy in melanoma - the role of BRAF, RAS and KIT mutations. *EJC Supplements*, 11(2):92–6, 2013.

[60] M. Davies and J. Gershenwald. Targeted Therapy for Melanoma - A Primer. *Surgical Oncology Clinics of North America*, 20(1):165–80, 2011.

[61] B.S. Kalal, D. Upadhya, and V. Ramanath Pai. Chemotherapy resistance mechanisms in advanced skin cancer. *Oncology Reviews*, 11(1):326, 2017.

[62] K. Chen, J. Valencia, J-P. Gillet, V. Hearing, and M. Gottesman. Involvment of ABC Transporters in Melanomagenesis and the Development of Multidrug Resistance of Melanoma. *Pigment Cell Melanoma Research*, 22(6):740–49, 2009.

[63] N.A. Frank, A. Margaryan, Y. Huang, T. Schatton, A.M. Waaga-Gasser, M. Gasser, M.H. Sayegh, W. Sadee, and M.H. Frank. ABCB5-Mediated Doxorubicin Transport and Chemoresistance in Human Malignant Melanoma. *Cancer Research*, 65(10):4320– 33, 2005.

[64] M. Chartrain, J. Riond, A. Stennevin, I. Vandenberghe, B. Gomes, L. Lamat, N. Meyer, J.E. Gairin, N. Guibaud, and J.P. Annereau. Melanoma Chemotherapy Leads to the Selection of ABCB5-Expressing Cells. *PLoS One*, 7(5):1–12, 2012.

[65] T. Schatton, G. Murphy, N. Frank, K. Yamaura, A.M. Waaga-Gasser, M. Gasser, Q. Zhan, S. Jordan, L. Duncan, C. Weishaup, R. Fuhlbrigge, T. Kupper, M. Sayegh, and M. Frank. Identification of cells initiating human melanomas. *Nature*, 451(7176):345–49, 2008.

[66] B. Ksander, P. Kolovou, B. Wilson, K. Saab, Q. Guo, J. Ma, S. McGuire, M. Gregory, W. Vincent, V. Perez, F. Cruz-Guilloty, W. Kao, M. Call, B. Tucker, Q. Zhan, G. Murphy, K. Lathrop, C. Alt, L. Mortensen, C. Lin, J. Zieske, M. Frank, and N. Frank. ABCB5 is a limbal stem cell gene required for corneal development and repair. *Nature*, 511(7509):353–57, 2014.

[67] N. Kugimiya, A. Nishimoto, T. Hosoyama, K. Ueno, T. Enoki, T-S. Li, and K. Hamano. The c-MYC-ABCB5 axis plays a pivotal role in 5-fluorouracil resistance in human colon cancer cells. *Journal of Cellular and Molecular Medicine*, 19(7):1569–81, 2015.

[68] B. Wilson, T. Schatton, Q. Zhan, M. Gasser, J. Ma, K. Saab, R. Schanche, A-M. WaagaGasser, J. Gold, Q. Huang, G. Murphy, M. Frank, and N. Frank. ABCB5 identifies a therapy-refractory tumor cell population in colorectal cancer patients. *Cancer Research*, 71(15):5307–16, 2011.

[69] P. Cheung, T. To Cheung, C. Wai Yip, L. Ng, S. Wai Fung, C. Mau Lo, S. Tat Fan, and S. Tim Cheung. Hepatic cancer stem cell marker granulin-epithelin precursor and *β*-catenin expression associate with recurrence in hepatocellular carcinoma. *Oncotarget*, 7(16):21644–57, 2016.

[70] H. Farawela, M. Khorshied, N. Kassem, H. Kassem, and H. Zawam. The clinical relevance and prognostic significance of adenosine triphosphate ATP-binding cassette (ABCB5) and multidrug resistance (MDR1) genes expression in acut leukemia: and

Egyptian study. *Journal of Cancer Research and Clinical Oncology*, 140(8):1323–30, 2014.

[71] M. Yang, W. Li, D. Fan, Y. Yan, X. Zhang, Y. Zhang, and D. Xiong. Expression of ABCB5 gene in hematological malignances and its significance. *Leukemia and Lymphoma*, 53(6):1211–15, 2012.

[72] Q. Guo, T. Grimming, G. Gonzalez, A. Giobbie-Hurder, G. Berg, N. Carr, B. Wilson,
P. Banerjee, J. Ma, J. Gold, B. Nandi, Q. Huang, A. Waaga-Gasser, C. Lian, G. Murphy, M. Frank, M. Gasser, and N. Frank. ATP-bining cassette member B5 (ABCB5) promotes tumor cell invasiveness in human colorectal cancer. *The Journal of Biological Chemistry*, 293(28):11166–78, 2018.

[73] B. Wilson, K. Saab, J. Ma, T. Schatton, P. Putz, Q. Zhan, G. Murphy ad M. Gasser, A. Waaga-Gasser, N. Frank, and M. Frank. ABCB5 maintains melanoma-initiatin cells through a pro-inflammatory cytokine signaling circuit. *Cancer Research*, 74(15):4196– 4207, 2014.

[74] J. Lin, M. Zhang, T. Schatton, B. Wilson, A. Alloo, J. Ma, A. Qureshi, N. Frank, J. Han, and M. Frank. Genetically determined ABCB5 functionality correlates with pigmentation phenotype and melanoma risk. *Biochemical and Biophysical Research Communications*, 436(3):536–42, 2013.

[75] S. Wang, L. Tang, J. Lin, Z. Shen, Y. Yao, W. Wang, S. Tao, C. Gu, J. Ma, Y. Xie, and Y. Liu. ABCB5 promotes melanoma metastasis through enhancing nf-*κ*b p65 protein stability. *Biochemical and Biophysical Research Communications*, 492(1):18–26, 2017.

[76] K. Moitra, M. Scally, K. McGee, G. Lancaster, B. Gold, and M. Dean. Molecular Evolutionary Analysis of ABCB5: The Ancestral Gene Is a Full Transporter with Potentially Deleterious Single Nucleotide Polymorphisms. *PLoS One*, 6(1), 2011.

[77] M. Krauthammer, Y. Kong, A. Bacchiocchi, P. Evans, N. Pornputtapong, C. Wu, J. McCusker, S. Ma, E. Cheng, R. Straub, M. Serin, M. Bosenberg, S. Aryian, D. Narayan, M. Sznol, H. Kluger, S. Mane, J. Schiessinger, R. Litton, and R. Halabn. Exome sequencing identifies recurrent mutations in NF1 and RASopathy genes in sun-exposed melanomas. *Nature Genetics*, 47(9):996–1002, 2015.

[78] G. Sana, J. Madigan, and J. Gartner. Exome sequencing of ABCB5 identifies recurrent melanoma mutations that result in increased proliferative and invasive capacities. *In preparation*.

[79] Y. Huang, P. Anderle, K. Bussey, C. Barbacioru, U. Shankavaram, Z. Dai, W. Reinhold, A. Papp, J. Weinstein, and W. Sadee. Membrane Transporters and Channels: Role of the Transportome in Cancer Chemosensitivity and Chemoresistance. *Cancer Research*, 64:4294–4301, 2004.

[80] P. Hsu, E. Lander, and F. Zhang. Development and applications of CRISPR-Cas9 for genome engineering. *Cell*, 157(6):1262–78, 2014.

[81] Y. Mei, Y. Wang, H. Chen, Z. Sheng Sun, and X-D. Ju. Recent Progress in CRISPR/Cas9 Technology. *Journal of Genetics and Genomics*, 43:63–75, 2016.

[82] T. Karvelis, G. Gasiunas, and V. Siksnys. Methods for decoding Cas9 protospacer adjacent motif (PAM sequences: A brief overview. *Methods*, pages 121–22, 2017.

[83] F. Ran, P. Hsu, J. Wright, V. Agarwala, D. Scott, and F. Zhang. Genome engineering using the CRISPR-Cas9 system. *Nature Protocols*, 8(11):2281–2308, 2013.

[84] Z. Ratan, Y-J. Son, M. Haidere, B. Uddin, A. Yusuf, S. Zaman, J-H. Kim, L. Banu, and J. Cho. CRISPR-Cas9: a promising genetic engineering approach in cancer research.
Therapeutic Advances in Medical Oncology, 10:1–15, 2018.

[85] C. de Duve, B. Pressman, G. Gianetto, R. Wattiaux, and F. Appelmans. Tissue fractionation studies. intracellular distribution patterns of enzymes in rat-liver tissue. *Biochemical Journal*, 60(4):604–17, 1955.

[86] O. Boussif, F. Lezoualc'h, M. Zanta, M. Mergny, D. Scherman, B. Demeneix, and J. Behr. A versatile vector for gene and oligonucleotide transfer into cells in culture and in vivo: polyethylenimine. *Proceedings of the National Academy of Sciences of the United States of America*, 92(16):7297–301, 1995.

[87] A. Akinc, M. Thomas, A. Klibanov, and R. Langer. Exploring polyethyleniminemediated DNA transfection and the proton sponge hypothesis. *The Journal of Gene Medicine*, 7(5):657–63, 2005.

[88] D. Desplancq, G. Freund, S. Conic, AP. Sibler, P. Didier, A. Stoessel, M. Oulad-Abdelghani, M. Vigneron, J. Wagner, Y. Mély, B. Chatton, L. Tora, and E. Weiss. CRISPR/Cas9-mediated gene disruption using jetPRIME. *Experimental Cell Research*, 342:145–58, 2016.

[89] Y. Song, L. Lai, and Z. Li. Large-scale genomic deletions mediated by CRISPR/Cas9 system. *Oncotarget*, 8(4):5647, 2017.

[90] J-P. Zhang, X-L. Li, A. Neises, W. Chen, L-P. Hu, G-Z. Ji, J-Y. Yu, J. Xu, W-P. Yuan, T. Cheng, and X-B. Zhang. Different Effects of sgRNA Length on CRISPR-mediated Gene Knockout Efficiency. *Nature Scientific Reports*, 6(28566), 2016.

[91] S. Tsai and J. Joung. Defining and improving the genome-wide specificities of CRISPRCas9 nucleases. *Nature*, 17:300–22, 2016.

[92] X-H. Zhang, L. Tee, X-G. Wang, Q-S. Huang, and S-H. Yang. Off-target Effects in CRISPR/Cas9-mediated Genome Engineering. *Molecular Therapy - Nucleic Acids*, 4:e264, 2015.

[93] A. Gear and J. Bednarek. Direct counting and sizing of mitochondria in solution. *The Journal of Cell Biology*, 54(2):325–45, 1972.

[94] A. Calcabrini, S. Meschini, A. Stringaro, M. Cianfriglia, G. Arancia, and A. Molinari. Detection of P-glycoprotein in the Nuclear Envelope of Multidrug Resistant Cells.
Journal of Molecular Histology, 32(10):599–606, 2000.

[95] W. Szaflarski, P. Sujika-Kordowska, R. Januckowski, K. Wojtowicz, M. Andrzejewska, M. Nowicki, and M. Zabel. Nuclear localization of P-glycoprotein is responsible for protection of the nucleus from doxorubicin in the resistant LoVo cell line. *Biomedicine and Pharmacotherapy*, 67(6):497–502, 2013.

[96] O. Menyhart, H. Harami-Papp, S. Sukumar, R. Schäfer, L. Magnani, O. de Barrios, and B. Gyorffy. Guidelines for the selection of functional assays to evaluate the hallmarks of cancer. *Biochimica et Biophysica Acta*, 1866(2):300–19, 2016.

Supplementary Material

Figure S1: Results of the sequencing of the PCR product for the detection of the 53 kb deletion. The sequencing of the PCR product confirms the rattachment between both exons 4 and 15, following the cleavage by the CRISPR/Cas9 system. The exon 4 (purple) is deleted from 28 nucleotides and directly followed by a part of the exon 15 (red) deleted from 23 nucleotides. The results of the sequencing have been analyzed with the NCBI BLAST tool.

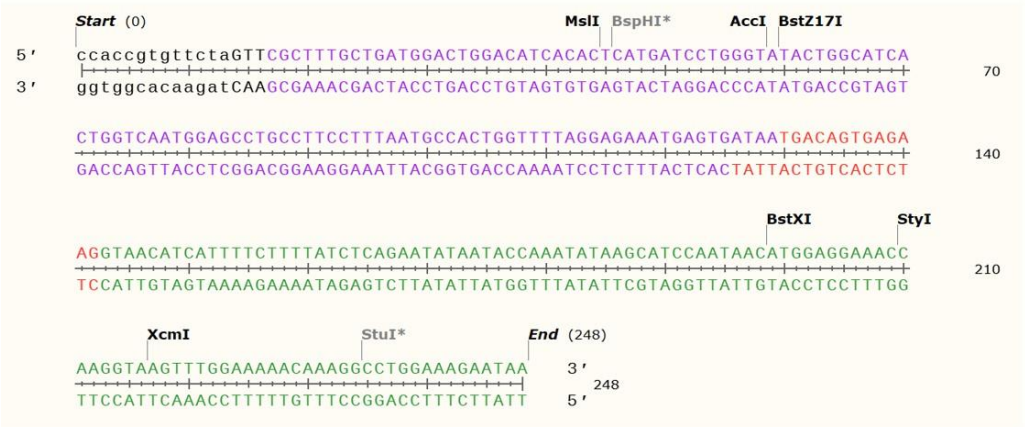

Figure S2: Results of the sequencing of the PCR product for the detection of the 125 kb deletion. The sequencing of the PCR product confirms the rattachment between both exons 4 and 27 after the cleavage by the CRISPR/Cas9 system. The exon 4 (purple) is deleted from 38 nucleotides and directly followed by the last 17 nucleotides of exon 27 (red) and the sequence of intron (green). The results of the sequencing have been analyzed with the NCBI BLAST tool.